Marine Geology
December 2004; 213(1-4) : 291-321
http://dx.doi.org/10.1016/j.margeo.2004.10.011

Triggering mechanisms of slope instability processes and sediment failures on continental margins: a geotechnical approach

N. Sultan[a*], P. Cochonat[a], M. Canals[b], A. Cattaneo[c], B. Dennielou[a], H. Haflidason[d], J.S. Laberg[e], D. Long[f], J. Mienert[e], F. Trincardi[c], R. Urgeles[b], T.O. Vorren[e] and C. Wilson[f]

[a]IFREMER, Plouzané, France
[b]University of Barcelona, Barcelona, Spain
[c]IGM, Bologna, Italy
[d]University of Bergen, Bergen, Norway
[e]University of Tromsø, Tromsø, Norway
[f]British Geological Survey, Edinburgh, UK

*: Corresponding author : Tel.: +33 2 98 22 42 59; fax: +33 2 98 22 45 70. nabil.sultan@ifremer.fr

Abstract:

The Costa target areas exhibit the variability of slope instabilities needed to improve our understanding of sediment physical and mechanical properties in areas prone to sliding. That is why in this project, we have analysed the different slope failures events from different parts of the Costa target areas, which reflect diverse triggering mechanisms. The aim of the first part of this study was to identify the geotechnical response of the sediment to different external mechanisms (earthquake, rapid sedimentation and gas hydrate melting). We have focused on the relation between external mechanisms and the consequence change in the in-situ stress state and the physical, mechanical, and elastic properties of the sediment.
In the second part of the paper, the geotechnical properties of the sediment from different Costa areas are presented. Comparison between observed geotechnical properties and the theoretical behaviour was done in order to improve our understanding of the origin of the different observed slides.

Keywords: earthquake; hydrate; sedimentation; sensitivity; slope instability

ABSTRACT

The Costa target areas exhibit the variability of slope instabilities needed to improve our understanding of sediment physical and mechanical properties in areas prone to sliding. That is why in this project we have analysed the different slope failures events from different parts of the Costa target areas, which reflect diverse triggering mechanisms. The aim of the first part of this study was to identify the geotechnical response of the sediment to different external mechanisms (earthquake, rapid sedimentation and gas hydrate melting). We have focused on the relation between external mechanisms and the consequence change in the in-situ stress state and the physical, mechanical, and elastic properties of the sediment.

In the second part of the paper the geotechnical properties of the sediment from different Costa areas are presented. Comparison between observed geotechnical properties and the theoretical behaviour was done in order to improve our understanding of the origin of the different observed slides.

Keywords: earthquake, hydrate, sedimentation, sensitivity, slope instability.

1 INTRODUCTION

A triggering mechanism is an external stimulus that initiates the slope instability process. According to Locat and Lee (2002), in marine domain, examples of triggering mechanisms include 1) oversteepening, 2) seismic loading, 3) storm-wave loading, 4) rapid sediment accumulation and under-consolidation, 5) gas charging, 6) gas hydrate dissociation, 7) low tides, 8) seepage 9) glacial loading and 10) volcanic island processes. These mechanisms can be considered as short-term triggers. In addition to the trigger mechanisms, causal factors can contribute to instability but may not initiate failure. Those causal factors are considered as long-term triggers. In marine domain, the list of causal factors can include the slope angle, mass-movement history and unloading. Unloading can be very critical in the case of gassy

sediment. Human activities such as slope loading can either be triggering mechanisms or causal factors depending on other slope conditions.

The primary focus of this study is to identify the relation between triggering mechanisms and causal factors on one hand and the stress state and geotechnical parameters on the other hand. In the costa project, from south to north, the working areas cover three sectors of the European continental slope:

1- Adriatic margin;

2- Western Mediterranean margin;

3- NE Atlantic margin.

Table 1 presents all the possible trigger mechanisms for the origin of the observed slope failures in the Costa target areas.

2 IN SITU STRESS STATE AND SEDIMENT BEHAVIOUR IN RESPONSE TO SOME EXTERNAL MECHANISMS

2.1 Sediment behaviour in response to a cyclic loading (earthquake)

Under cyclic loading, the sediment dynamic behaviour is influenced by the intensity and duration of the cyclic loading and the state of the sediment (the grain size distribution, the presence or absence of a clay fraction, and the degree of saturation). Cyclic loading may induce degradation of soft clays (see for instance Pestana et al. 2000) such as those found in many marine deposits. Indeed, the cyclic loading is associated with 1) degradation of the sediment stiffness 2) degradation of the shear strength and 3) increase in pore pressure during cyclic loading. On the other hand, when loose, saturated granular sediment is exposed to strong earthquake ground shaking the grains compact, squeeze together, and take up less space. Since the duration of the cyclic loading is too short to ensure the drainage of water, a decrease in the effective confining stress and a consequent increase of equal magnitude in the

pore water pressure will occur. When the sand is loose enough and the magnitude of the cyclic shear stress is high enough, the vertical effective stress drops to zero (see for instance Ishihara 1985). For sands and silty sands, this phenomenon is known as sediment liquefaction. Earthquakes may trigger a phenomenon in certain clays that produces effects similar to liquefaction in water-saturated sand. For clayey sediment, sensitivity can be at the origin of a significant loss of strength. Extremely sensitive clays, which appear to be quite strong, have the tendency to change from a relatively stiff condition to a liquid mass when it is disturbed.

Very hazardous cases are usually associated with liquefaction of saturated cohesionless sediments during earthquakes. The liquefaction failure over gentle slope enhances lateral spreading, ground settlement and sometimes generates sand boils (see for instance Varnes 1978).

The assessment of the potential for triggering or initiation of sediment liquefaction has been a problem of major concern since the early 1960s. For silty and clayey sands, Andrews and Martin (2000), based on the database of Seed et al. (1984, 1985), define a criterion for liquefaction susceptibility (Table 2). In order to evaluate the liquefaction potential, two primary seismic variables are required. These variables are the level of cyclic stress induced by the earthquake on a sediment layer, expressed in terms of cyclic stress ratio (CSR), and the capacity of a sediment layer to resist liquefaction, expressed in terms of cyclic resistance ratio (CRR). Seed and Idriss (1971) formulated the following equation for calculating CSR:

$$CSR=\frac{\tau_{av}}{\sigma'_{v0}}\approx 0.65\left(\frac{a_{\max}}{g}\right)\left(\frac{\sigma_{v0}}{\sigma'_{v0}}\right)r_d \qquad [1]$$

where a_{max} is the peak horizontal acceleration at the surface of the sediment deposit during an earthquake, g is the gravitational acceleration, σ_{v0} and σ'_{v0} are total and effective overburden stress, respectively; and r_d is a stress reduction factor (see for instance Seed et al. 2001).

Evaluation of the cyclic resistance ratio (CRR) has developed along two specific areas of research: methods based on the results of laboratory tests, and methods based on in situ tests

and field observations of liquefaction behaviour in past earthquakes. In laboratory testing, the number of shear stress cycles to achieve liquefaction, is the basis for expressing the resistance of sediment to the initiation of liquefaction. Liu et al. (2001) developed empirical regression equations that can be used to evaluate the number of uniform shear stress cycles of earthquake shaking as a function of magnitude, site-source distance, site condition, and near-fault rupture directivity effects (Figure 1). Therefore, based on experimental tests and the number of uniform shear stress cycles evaluated from Liu et al. diagram (Figure 1), it is possible to identify the cyclic resistance ratio of the sediment, CRR. The potential for liquefaction can then be evaluated by comparing the earthquake loading (CSR) with the liquefaction resistance (CRR) - this is usually expressed as a factor of safety against liquefaction

$$FS=\frac{CRR}{CSR} \quad [2]$$

A factor of safety greater than one indicates that the liquefaction resistance exceeds the earthquake loading, and therefore that liquefaction would not be expected.

2.2 Sediment behaviour in response to a high sedimentation rate

In a normal hydrostatically pressured geological formation, the sediment is permeable and the fluid can communicate through the different layers. The pore water is free to escape during consolidation; thus the fluid pressure is hydrostatic. For over-pressurized layers, the permeability of the sediment is low which prevents or at least restricts the fluid circulation. The increase of sediment loading generated by sedimentation is transferred in part from the sediment matrix to the water. Thus, the pore water partially supports the overburden pressure, which prevents the pores from collapsing under the weight of the overburden. The normal consolidation phenomenon is retarded and the sediment is in an under-consolidated state. When the forces caused by the fluid pressure gradients exceed the confining stress then the sediment will boil or become quick. From the sedimentation rate, the porosity, the

permeability and the bulk unit weight of the sediment, it is possible to quantify by a back analysis the evolution of the excess pore pressure and the stress state over the geological formation. For that, the principle of the effective stress that defines the effective stress in porous media (σ'_v) as the difference between the total stress (σ_v) and pore fluid pressure (u) is used (eq. 3).

$$\sigma'_v = \sigma_v - u \quad [3]$$

In equation 3, the pore fluid pressure u is the sum of the hydrostatic pressure ($p_w gz$) and the excess pore pressure (Δu).

$$u = \Delta u + \rho_w gz \quad [4]$$

The link between the void ratio e and the vertical effective stress is considered through the following equation:

$$e = e_0 - \lambda ln\left(\frac{\sigma'_v}{\sigma'_0}\right) \quad [5]$$

where e_0 is a reference void ratio at a reference vertical effective stress σ'_0, and λ is the compression index.

The process of consolidation is directly related to the rate of excess pore pressure dissipation and the rate of sedimentation. The key equation used to evaluate the evolution of the excess pore pressure during the sedimentation process is given by:

$$\frac{\partial u}{\partial t} = \left[\frac{k(1-\phi)^2}{S_t \mu}\right]\nabla^2 u + \left[\frac{\phi\beta}{S_t(1-\phi)}\right]\frac{\partial \sigma_v}{\partial t} \quad [6]$$

where ϕ is the porosity, k is the intrinsic permeability, μ is the fluid viscosity, β is the bulk compressibiliy and S_t is the storage coefficient. S_t assumes the solid grains as incompressible and is defined by the following equation:

$$S_t = \frac{\phi\beta}{(1-\phi)} + \phi\beta_f \quad [7]$$

where β_f is the fluid compressibility.

In order to evaluate the over-consolidation state of the sediment layers from the different Costa target areas, the system of equations (3 through 7) is solved numerically applying a finite difference model. The upper model boundary is a moving boundary due to continuous sedimentation. As an example, three different sedimentation rates of 0.1 m/ky, 0.2 m/ky and 0.4 m/ky were tested. According to the sedimentation rate the age of the sediment column varies between 2.5 m.y. (for a rate of 0.4 m/ky) and 10 m.y. (for a rate of m/ky). The simulation results are presented in Figure 2, which show clearly the dependence of the excess pore pressure on the sedimentation rate.

Hydrofracturing could be generated when the difference between the fluid pressure and least principal (confining) stress becomes close to zero. On the other hand, and contrary to what is mentioned by several authors (see for instance Henriet et al. 1991, Cartwright et al. 1994 among other), hydrofracturing cannot generate polygon faults. Indeed hydrofracturing generates only Mode I fractures (displacement perpendicular to fracture) and is not directly relevant to the formation of shear fractures or faults (Watterson et al. 2000).

2.3 Sediment behaviour in response to gas hydrates melting.

Gas hydrate cements sediment and therefore, it modifies significantly the sediment strength; its formation and breakdown may influence the occurrence and location of submarine landslides. The upper limit of the gas hydrate stability zone (pinch-out) where expulsion of free gas is expected can lead to sediment slope instabilities and can be considered as a potential cause of geohazard.

Parameters that affect gas hydrate formation include temperature, pore pressure, gas chemistry, and pore-water salinity. Any change in the equilibrium parameters may trigger seabed instability by converting the hydrate to gas plus water, causing significant weakening of the sediment, and generating a rise of pore pressure. The excess pore pressure generated by the hydrate melting depends on the solubility of the dissolved gas and on the ratio of the gas

to water in the hydrate phase. The ratio of methane to water in the hydrate phase are around 150 times greater than the ratio of methane to water in the aqueous solution. Therefore, the melting of the hydrate phase will generate a huge quantity of methane, which is much higher than the solubility of the dissolved gas in the aqueous solution. At short term, and under the assumption of no gas diffusion and no volume change of the sediment, it is possible to evaluate the excess pore pressure generated by the hydrate melting using a state equation (see Sultan et al., this volume).

In addition, gas hydrate dissociation can induce free gas within the marine sediment. Gassy sediment, which contains relatively large amounts of gas dissolved in the pore fluid is hazardous when is unloaded in undrained conditions (see for instance Sobkowicz and Morgenstern 1984 and Vanoudheusden et al. this volume).

3 GEOTECHNICAL DATA FROM DIFFERENT SLIDING AREAS

The aim of this study is to identify the possible trigger mechanisms at the origin of the observed slope failures in the Costa target areas. Thus, different geotechnical parameters were identified from the different areas by carrying out in situ and laboratory measurements (Table 3).

Three types of laboratory tests were used in order to identify the relevant geotechnical parameters (Table 3): 1) Saturated sediment submitted to static loading: to identify the basic classical geotechnical data; 2) Gassy sediment submitted to static loading: to identify the behaviour of gassy sediment in relation with gas hydrate and gas flow and 3) Saturated sediment submitted to cyclic loading: to determine the build up pore pressure generated by an earthquake and to identify the degradation of the stiffness and the shear resistance of the sediment during an earthquake. Two types of in-situ measurements were planned (Table 3): 1) Long term monitoring of the in-situ pore pressure: to determine the build up pore pressure

generated by an earthquake and 2) In situ measurement using the penetrometer: to identify the in-situ physical and mechanical parameters of unremoulded sediment.

In order to identify the relation between earthquake shock and the excess pore pressure, the University of Tromsø developed with Geotek Ltd. an Ocean Floor Observatory (OFOS) aimed at measuring simultaneously both seismicity at the seafloor and pore pressure within the upper 4 m of sediment. The OFOS was deployed in a slide-prone and seismically active area of the Adriatic Sea about 4 nautical miles offshore the port of Ortona (Italy) on May 16th 2001 (deployment site coordinates were 42 25.1701'N, 14 26.4872'E referred to WGS84 datum, in 31.4 m water depth - Figure 3) and recovered on April 15th 2002. Several earthquakes occurred during the deployment, at least 3 events in the vicinity of the site exceeded Richter Magnitude 4 and some were recorded by the Ocean Bottom Seismimeter that collected a total of 4 Gbytes of seismic data. Unfortunately, the long term pore pressure measurement using OFOS failed due to a leakage in the recording unit.

3.1 Central Adriatic shelf

3.1.1 Geological setting

During the late Holocene, a progradational mud wedge up to 35 m in thickness deposited along the western side of the Adriatic basin. This late-Holocene mud wedge has an overall clinoform geometry with a submerged offlap break in ca. 25 m water depth and deposited on a flat surface dipping ca. 0.2°, whereas the average gradient of the foresets is 0.5°. The mud wedge is composed of a basal unit (ca. 1 m thick) overlain by three sigmoidal prograding units; the base of the mud wedge is a regional downlap surface that represents the time of maximum sea level highstand dated ca. 5.5 ka BP (Correggiari et al., 2001; Cattaneo et al., 2003a).

Over large areas (more than 250 km parallel to the coast, between ca 30 and 110 m water depth), the basal unit is acoustically transparent and topped by a discontinuous reflector showing lateral variations in seismic amplitude, likely because of the presence of shallow gas and fluid escape (Trincardi et al., this volume). In these areas, deformation affects the whole stratigraphic section of the mud wedge or selective sub-units (Correggiari et al., 2001; Cattaneo et al., 2003b). Sediment deformation occurs as seafloor and subsurface undulations (in water depth of ca 30 to 70 m) with strikes that are sub-parallel to the regional bathymetric contour (Correggiari et al., 2001; Cattaneo et al., this volume), or as small-scale mud reliefs with preferred crest orientations that are perpendicular to regional contours (Cattaneo et al., 2003b; Marsset et al., 2003).

If compared to other areas of the COSTA Project, the central Adriatic represents an end member where: a) several kinds of deformation are restricted to the stratigraphic section above a common key stratigraphic surface, the mfs; b) sediment deformation occurs in close association to the presence of shallow gas or fluid escape features on the shelf; c) sediment deformation with limited displacement did not evolve into disintegration and flow. In order to evaluate the role of the basal unit as a potential weak layer for sediment deformation, we sampled it through acoustically-transparent mud reliefs with 10- or 15-m long piston cores.

3.1.2 Geotechnical characterisation

Two cores provided samples for laboratory oedometer tests (Figure 3 and Table 4). Both cores were recovered with a 10-cm diameter piston corer, mounted with a 10 and 15 m barrel respectively: COS01-29 (945 cm long, with sediment compaction due to sampling of ca 92%) and COS01-31 (1447 cm long, compaction of ca. 96%). The careful positioning of the cores obtained with DGPS, a swath bathymetric map and Chirping-while-coring technique allowed to hit the targeted mud reliefs and core through them to reach beyond the mfs. The oedometer tests were conducted to identify some geotechnical parameters (preconsolidation pressure,

compression index and coefficient of consolidation), which are necessary to describe the 1-dimensional compression behaviour of the sediment. Figure 4 presents the oedometer compression curves of the four samples from cores COS01-29 and COS01-31. The determination of the preconsolidation pressure from the oedometer curves shows a high under-consolidated sediment. Indeed, the over-consolidation ratio is comprised between 0.37 and 0.41 for core COS01-29 and between 0.26 and 0.27 for core COS01-31 (Table 4). The compression index λ is comprised between 0.151 for the sample A3 and 0.187 for the sample A1 (Table 4). During the oedometer tests, a measurement of the permeability coefficients was carried out. From the experimental data, it was possible to define an analytical expression of the permeability coefficient as a function of the void ratio (eq. 8).

$$k(m/s)=\exp(1.65e-23.90) \quad [8]$$

3.1.2.1 Cyclic tests

In addition to the oedometer geotechnical tests, 4 cyclic tests were carried on samples from the Adriatic slope and at different loading amplitudes (Figure 3- Table 5). The aim of these cyclic tests was to compare the pore pressure build-up generated within the basal unit (samples A5 and A6) to the one generated in the surrounding sediment.

The particle size distribution of the two samples from the basal unit shows a clay content of 34 % for A5 (core COS01-29) and 38% for A6 (core COS01-31). For the two cores, the sediment can be considered as silty clay.

Figure 5 and Figure 6 present two triaxial tests carried out on samples A6 (basal unit) and A8. For the cyclic test, the change of the following three parameters as a function of the number of cycles N is presented:

1) The Cyclic Resistance Ratio (CRR) which is equal to the half applied cyclic shear ($\Delta q/2$) divided by the initial effective confining pressure (σ'_{30})
2) the vertical strain

3) the excess pore pressure generated by the cyclic loading and normalised with respect to the initial effective confining pressure (σ'_{30}).

For the sample A5, the test was stopped before liquefaction after 25 uniform cycles. For the sample A6, liquefaction (i.e. the condition when the excess pore pressure is equal to the initial effective confining pressure) was reached after 78 uniform cycles (Figure 5). For the sample A6, the liquefaction was abrupt and not progressive as it is usually observed from triaxial cyclic tests. On the other hand, and although the high applied cyclic shear amplitude on the sample A8 with respect to the load applied on sample A6 (Table 5), no liquefaction was observed after 200 uniform cycles (Figure 6).

3.1.3 Results and discussion

In order to evaluate the over-consolidation state of the sediment from the Adriatic area, the system of equations (3 through 7) was solved numerically applying a finite difference model. From this area, a correlation based on recognition of physical surfaces on seismic profiles and of magnetic susceptibility logs (Correggiari et al., 2001, Cattaneo et al., 2003a) allows to identify an average Sediment Accumulation Rate (SAR) for the section above the maximum flooding surface (mfs) dated ca. 5.5 ka BP; and for the section above the base of the Little Ice Age unit, dated ca. 0.5 ka BP (Figure 3); for example, in core COS01-31 the mfs was estimated at 9.40 m bsf, whereas the base of the Little Ice Age at 2.80 m. In addition to the Sediment Accumulation Rate data, the compression index and the permeability coefficients identified form the oedometer compression tests (Figure 4) were used to evaluate the excess pore pressure generated during the last 5.5 ka. In Figure 7 the simulation results of the vertical effective stress, the excess pore pressure and the porosity versus depth are presented. The excess pore pressure generated by the sedimentation accumulation during the last 5.5 ka corresponds to 6% of the hydrostatic pressure at the level of the maximum flooding surface (mfs) and is low to be considered alone as a causal mechanism for the observed mud reliefs.

Indeed, for a critical hydraulic gradient, the sediment is in quick condition when the vertical effective stress drops to zero, which was not the case under the sedimentation accumulation in the Adriatic area (see Figure 7).

Four cyclic tests were carried on samples from the Adriatic slope and at different loading amplitudes (Table 5). The aim of these cyclic tests was to compare the build-up pore pressure generated within the basal unit (samples A5 and A6) to the one generated in the surrounding sediment. Preliminary results show that sediment from the basal unit is more susceptible to liquefaction than the surrounding sediments. It is important to mention that liquefaction was observed on only one sample from the basal unit and it was abrupt which is not common in this type of cyclic triaxial test. Additional triaxial cyclic tests on samples from the basal unit must be carried out in order to be certain of this feature of behaviour.

3.2 Afen Slide

3.2.1 Geological setting

The West Shetland margin is a site of extensive margin progradation during Plio-Pleistocene times, with mid – late Pleistocene sedimentation influenced by icesheets that regularly extended to the shelf break (Stoker et al., 1993). The seafloor shows only one major recent slide, the Afen Slide, but there is evidence of older instability (Long et al 2003). The Afen Slide is between 830 and 1150 mbsf, approximately 13 km length and up to 4 km wide, excavating less than 20 m of sediment. These are typically very soft to soft, glaciomarine muds and silts reworked by alongslope currents flowing from the northeast.

3.2.2 Geotechnical measurements

All the measurements of shear strength used in this study come from split core samples using the hand vane or fall cone. The cores taken from inside the slide area show much greater variability than those from the undisturbed sediments outside the slide (Figure 8) (also Wilson

et al this volume). The variability of the disturbed material may be explained by the chaotic nature of deposition with individual clasts in various states of over or under-consolidation present within the matrix of reworked material from the debris flow. The measurements of higher average unit weight (17.5 kN/m^3 compared to 16.9 kN/m^3) and lower average moisture content (46% compared to 56%) for the material inside the slide area is consistent with this interpretation.

3.2.3 Results and discussion

From high resolution deep tow boomer data it has been shown (Wilson, et al., 2003) that the Afen Slide failed along a surface of rupture that closely matches the seismo-acoustic layering of the slope sediments. Several of these layers have been interpreted as sheeted sandy contourite deposits (Figure 9). It has also been shown that there are modern, well sorted sandy contourites at the level of the slide headwall (Masson 2001) and that it appears as though along slope depositional process have dominated in this region since at least the Elsterian (Stoker et al., 1993; 1994) thus making up the sediments involved in the Afen Slide.

From this data we reason that there may be layers of well sorted contouritic sands within the strata, although a +20 m core from outside the slide area would be necessary to confirm this. Apart from being inherently less coherent than clayey sediments, sandier sediments are also susceptible to liquefaction under dynamic loading. Rapidly creating not only a localised plane of weakness but also the potential for raising the pore pressure of the surrounding cohesive sediments. It is impossible to be certain in this case whether it was the short-term liquefaction of the sands or the secondary process of weakening the surrounding clayey sediments that provided the plane of weakness along which the slide did eventually fail. However work by Hobbs et al (1997) has shown that without some form of dynamic influence the area of the Afen Slide is stable.

Whilst seismicity is usually investigated or defined on a regional level the location of the epicentre is crucial in determining the likely effect of an earthquake of a given magnitude, in terms of slope instability (Keefer 1984). This makes the location of any potential areas of reactivation critical in the overall assessment of landslide hazard. Rumph et al (1993) integrate gravity and magnetic data to locate numerous transfer zones one of which (Victory) passes directly beneath the Afen Slide. Work by Muir-Wood (2000) and Stewart et al (2000) show how forces exerted by post-glacial rebound in northern Europe have been sufficient to control the crustal strain field and so the seismicity of the region. Thus, even though no data exists which could prove renewed movement along the Victory Transfer Zone at the time of slope failure there is a possibility that such an event occurred. The presence of a slide more than 30m below the seabed with similar proportions and just offset from the Afen slide may support the notion of reactivation of the transfer zone as this might provide a similar trigger for sediments with comparable properties (Figure 10). However, until more is known about the frequency/magnitude relationships of slope failures on this margin the true significance of the buried slide cannot be determined.

3.3 Big'95 Slide

3.3.1 Geological setting

The Ebro margin is located on the western side of the Valencia Trough, an early Miocene-Pleistocene extensional basin that lies between the Balearic Islands and the Iberian Peninsula in the NW Mediterranean. The Neogene sediments are characterized by a thick progradational sequence of mostly Pliocene to Pleistocene sediments overlying the Messinian unconformity (Clavell and Berastegui, 1991; Maillard et al., 1992).

In 1995 a major instability event in the form of a debris flow named BIG'95 (see Lastras et al., 2002) was mapped. The landslide involves 2,200 km^2 of seafloor (4 times the area of the

nearby island of Ibiza), and has a volume of 26 km^3. It affects the Ebro slope and base-of-slope at depths ranging from < 600 to 2000 m. Swath bathymetry data (Lastras et al. 2002, 2003) have shown an area of uneven topography in the Ebro slope with several main and secondary scars identified between 600 and 1200 m deep (Canals et al., 2000). Very high resolution seismic records show a large (2000 km^2) sediment body with transparent seismic facies forming the latest unit identifiable, thus indicating the event's youth. EM12 backscatter strength images (Lastras et al., 2002) show that the debris flow area consists of a pattern of low-backscatter patches and high backscatter topographically depressed lineations, representing respectively large blocks separated by the pathways of coarser sediment (Lastras et al., 2002). The large sediment blocks appear only between 1200 and 1550 m water depth, while coarse sediment paths are present all along the debris flow.

In the debris flow area and surroundings 7 piston cores, the results of which were presented by Urgeles et al. (2003), were obtained in 1997 (Figure 11). These cores, which penetrated between 3.1 and 8.6 metres, were logged using a Geotek MSCL for unit weight, porosity, magnetic susceptibility and P-wave velocity. The cores were later split on land and grain size, carbonate content, water content, specific weight, vane shear strength and remoulded shear strength analyses were performed. The cores are representative of both areas affected by the debris flow as well as areas immediately above the main failure scar that remained stable after the landslide took place.

3.3.2 Geotechnical characterisation

The logs and geotechnical analyses clearly differentiate an upper post-landslide unit, which shows a consistent pattern through all the studied sections with high-water contents (up to 80%), low densities, porosities and shear strengths and mean grain sizes of the order of 8-9 phi (very fine silts). The most distal cores show higher carbonate contents which indicates the influence of the Balearic margin to the east. The pre-landslide sediments are characterised by

water contents around 32% and unit weight between 16 and 17 kN/m^3. Those two properties and related ones, such as porosity, vary little along the core with a slight decrease in water content and porosity and increasing unit weight with depth. The cores obtained from areas not affected by the landslide (CLKS02 and CLKS03), show lower shear strengths than those obtained in the landslide mass. However, shear strength profiles show distinct features in these two cores. Core CLKS03, obtained on the open slope, upslope of the main scar, shows increasing shear strength with depth and very constant deviation and mean grain size, and magnetic susceptibility, while core CLKS02, obtained on the flank of a channel levee, shows little dependence of shear strength with depth and more variable mean grain size, grain size deviation and magnetic susceptibility. This difference probably arises from the sedimentation processes and rates on the open slope (mostly hemipelagic) compared to that of the levee, where accumulation from turbidite events occurs. Therefore, data from core CLKS02 probably indicate under-consolidated sediments.

The landslide sediments, i.e. those involved in the debris flow, have lesser amounts of water, and thus their unit weight is slightly higher. Water content is also slightly lower (by about 10%) than that of the pre-landslide sediments that have not been affected by the passage of the debris flow (cores CLKS02 and CLKS03). On the other hand, at the same consolidation stress, shear strength appears to be higher for the sediments involved into the debris flow than for those pre-dating the BIG'95. However, the remoulded shear strength is similar (around 5 kPa) for both the BIG'95 and pre BIG'95 sediments.

3.3.3 Results and discussion

The data obtained from the cores allow inferring that the location of the channel-levee deposits was probably an important factor controlling the location and morphology of the failure scar, and triggering of the debris flow (Urgeles et al., 2003). This is supported by the fact that under-consolidation seems to be present in core CLKS02 on the flank of a levee, and

it is believed that the higher sedimentation rates within this system result in higher pore pressures and lower shear strengths (this assumes that all cores represent sediments coming from the same source area, and therefore having very similar plasticity indexes). The above theory is also strengthen by the presence of channel ghosts within the headwall area (see also Lastras et al. 2002, 2003), with one of the channel ghosts being more or less parallel to the head-wall scar. Local uplift and oversteepening due to volcanic activity, as shown by seismic reflection profiling and morphology derived from the multibeam echosounder (Lastras et al., 2002) are also important factors to be considered.

3.4 Nice Slope

3.4.1 Geological setting

The Var river mouth exhibits a 100 m thick, aggradational-progradational, accumulation of Holocene sediments that overlies basal fluvial Pleistocene gravels. The Var delta consist of low-gradient delta-toe bottomsets, steep coarse to fine-grained delta front foresets affected by waves and a variety of gravity-driven processes, and topsets forming up to 80 m thick muddy laminites and thin peat interbeds (Figure 12) (Dubar and Anthony, 1995). Sedimentation patterns reflect the global Holocene sea-level rise and the interplay of a steep, high-relief hinterland, that has supplied clast sizes ranging from boulders to clay, and of the changing climate and vegetation during the Holocene (Dubar and Anthony, 1995). In the past century, reduction of channel width by embankments and the construction of several dams have severely affected the downstream sediment budget, by-passing the coastal zone and forcing the deposition on the continental slope (Dubar and Anthony, 1995). According to data from Dubar and Anthony (1995) and L'homer (1980) the average sedimentation rate was around 8.0 m/ka, during the sea-level rise between ~12 ka and ~7 ka BP ^{14}C, and about 3.5 m/ka during the slow sea-level rise between 7 ka and now. During this later period, the rate of

sediment input outpaced slow sea-level rise and subsidence and forced rapid progradation of fluvial deposits (Dubar and Anthony, 1995), leading to more reduced sedimentation rates on the nearshore shelf. The continental shelf is narrow (zero to few kilometres) and the continental slope is very steep with and average gradient of more than 11° (Cochonat et al., 1993). They are cut across by a succession of deep valleys alternating with spurs (Figure 13-a). A submarine slope failure occurred on October 1979 during the construction of the new Nice harbour. The submarine slope failure was considered as a typical shallow failure as has been surveyed by EM 1000 mapping (Bourillet et al, 1992). Figure 13-b shows the thickness of the slope failure determined from two sets of bathymetry data (before and after the 1979 accident). It is interesting to see that the deepest part of the slope failure is directly below the corner of the harbour extension.

Sediment cores located about 900 m and 500 m offshore of Nice airport, at the shelf break and on the continental slope (Figure 13-a) were studied in this work. Cores KGMO-04, KGMO-05, MD99-2468G and MD99-2469G were collected in the northern area on a bedded seismic facies identified on 3D Very High Resolution seismic, cores KGMO-03, KGMO-06, MD99-2470 and MD99-2471 were collected in the southern area on a transparent seismic facies. The sedimentary facies consist of brown to beige, clay to very fine sand laminates, similar to the facies describe by (Dubar and Anthony, 1995). They do not show any significant difference from a site to another. The lithology consists of detrital silty carbonates with some silty to fine sand quartz, few calcareous nannoplancton, occasional plant debris and very rare foraminifera. The light laminae are characterised by more abundant detrital carbonates. The laminae are horizontal on cores KGMO-03, KGMO-04 and MD01-2469G, they show a slight inclination (<5°) on cores KGMO-05 and KGMO-06 and a strong inclination (10°) on cores MD01-2468G, MD01-2470 and MD01-2471. Some small faults and deformation, probably related to local instability/slumping are visible on core MD01-2470.

Corrected AMS radiocarbon dating gave an age of 280±40 years BP ^{14}C (~ca 306 years BP) in core KGMO-03 at a depth of 352 cm, and an age of 810±40 years BP ^{14}C (~ ca 698 years BP) in core KGMO-04 at a depth of 302 cm. These ages yield sedimentation rates of 11.5 $m.ka^{-1}$ in the south part and of 4.3 $m.ka^{-1}$ in the north part. These sedimentation rates are in the same range as those calculated from Dubar & Anthony (1995).

The southern part of the area, close to the 1979 failure, is characterised by a ~10 metres thick homogeneous transparent seismic facies, by very high sedimentation rates (11.5 $m.ka^{-1}$), and by evidence of small scale faulting/deformation.

3.4.2 Geotechnical characterisation

The 8 cores collected from the Nice slope are characterized by sediment of high unit weight (between 16 kN/m^3 and 21 kN/m^3). From the undrained shear strength profiles (Figure 14-a and b), the sediment behaviour from the Nice slope can be divided into two parts:

- A linear increases of the undrained shear strength with depth corresponding to the transparent facies in the southern part of the slope (KGMO_03, KGMO_06, MD01-2470 and MD01-2471).
- A quasi-constant value of the undrained shear strength with depth in the northern area (KGMO_04, KGMO_05, MD01-2468 and MD01-2469).

However, the core MD01-2468G and MD01-2469G are characterized by a highly over-consolidated sediment within the upper 2 metres (Figure 14-b). The upper sediments from the Nice slope have a low sensitivity, most of the time less than 4 (Figure 14-a and b). The particle size distribution of the four samples shows that the clay content is comprised between 16 % for S4 and 26% for S1. For the four samples, the sediment can be considered as silty clay.

3.4.2.1 In-situ piezocone test

In 1994, Sols Mesures carried out along the Nice coast several in-situ piezocone tests (sols measures report - 1994). In Figure 15 is presented the corrected cone tip resistance (qt), differential pore water pressure (Δu), and sleeve friction (fs) profiles for the CPTU test pz11 (for location refer to Figure 13-a). The tip resistance profile shows peaks with a decrease of pore pressure; this is an indication of the presence of coarse-grained sediment. On the other hand, low values of the sleeve friction were observed at 45 mbsf (Figure 15). One of the main applications of the piezocone measurement is the determination of the stratigraphy and the lithology of buried sediment. Pore pressure is difficult to interpret in term of lithology. A soft clay as well as a contractive silt react to the penetration of the rod by generating a high pore pressure. On the other hand, a very stiff clay as well as a very dense silty clay or a dilative silt respond in the same way in term of pore pressure i.e. a low or even a negative pore pressure. Thanks to the combination of the 3 classical CPT sensors measurements (tip resistance, sleeve friction and pore pressure), it is possible to define a sediment classification chart (see for instance Campanella et al. 1982, Robertson et al. 1986, Robertson 1990 and Ramsey 2002 among others). In order to define the sediment type from the CPTU pz11 data, we have used in this work the diagram proposed by Ramsey 2002. Figure 15-d shows different facies associated to the pz11 cone penetration profile. It is interesting to see the existence, between 40 mbsf and 54 mbsf, of very sensitive clay. Under high deviatoric load (example: the embankement of the harbour extension), sensitive clay layer will be submitted to an important creep, which will decrease dramatically its resistance and may provoke slope failures. This hypothesis can be supported by the good concord between the maximum thickness of the failure surface (at around 50 mbsf - Figure 13-b) and the depth of the very sensitive clay layer (Figure 15-d).

3.4.2.2 Cyclic test

In addition to the classical static geotechnical tests, 10 cyclic tests were carried on samples from different areas of the Nice slope and at different loading amplitudes (Table 6). The aim of these cyclic tests was to identify 1) the build-up pore pressure generated within the different sediment layers during earthquake as a function of the loading amplitude and 2) to determine the degradation of the sediment stiffness and sediment resistance under the cyclic tests.

Triaxial tests were carried out on samples S4-1 and S4-3 from the Nice slope. For each test, changes in the Cyclic Resistance Ratio (CRR), the vertical strain and the excess pore pressure normalised with respect to the initial effective confining pressure as a function of the number of cycles N are presented in Figure 16. Figure 16 show that the liquefaction was reached after 30 uniform cycles. In addition to the cyclic triaxial tests carried out within this project, data from Sols Essais report (1994) (Table 7) on samples collected from the Nice slope between 37 m and 73 m depth were used in order to draw the variation of the CRR as a function of the cycles to liquefaction (Figure 17). A good agreement was observed between the data from literature (Sols Essais report - 1994) and the data from this work (Figure 17). The data from the Nice slope is presented together with the cyclic resistance of the Hostun sand (reference sand well studied in laboratory – see for instance Flavigny et al. 1990) with a relative density of 70 % (Figure 17). The cyclic resistance of the sediment from the Nice slope is high with respect to the Hostun sand (Dr=70%).

3.4.3 Results and discussion

To evaluate the liquefaction potential of the sediment layers from the Nice slope, the standard safety factor method has been used (equations 1 and 2, Figure 1 and Figure 17). The liquefaction potential has been evaluated for an earthquake of M=6.5. For a given PGA (Peak Ground Acceleration) the liquefaction potential for the different sediment layers from the

Nice slope is evaluated. As illustrated in Figure 18, the factor of safety against liquefaction is always greater than one. Indeed, the cyclic stress induced by earthquake (for PGA=0.5, 1 and 1.5 m/s²) is lower than the cyclic stress required to initiate liquefaction (Figure 18). From Figure 17 and Figure 18, we can conclude that the liquefaction potential is low on the Nice site due to lack of loose sediments. It is important to mention that the 1979 landslide on the Nice slope was not triggered by earthquake. The slope failure was generated after an exceptionally heavy rainfall and river discharge. This last observation reinforces the hypothesis of rapid accumulation or seepage of fresh water as a distinct or simultaneous possible trigger mechanisms at the origin of the Nice slope failure (Table 1). The very high sedimentation rate (11.5 $m.ka^{-1}$ in the south part and of 4.3 $m.ka^{-1}$ in the north part) in the area can defend this last hypothesis. However, in the absence of in-situ monitoring of the excess pore pressure it is difficult to evaluate the consequence of the seepage of fresh water on the slope stability over the Nice area.

The last possible trigger mechanism related to human activity cannot be neglected. Indeed, the submarine slope failure occurred on October 16th 1979 during the construction of the Nice harbour. A preliminary evaluation of the slope stability in the Nice area under the static gravitational loading carried out by Sultan et al. (2001) shows that failure condition (FOS<1) is reached at several local sections around the Nice airport at different depths. Besides, the good concord between the maximum thickness of the failure surface (at around 50 mbsf - Figure 13-b) below the harbour extension and the depth of the very sensitive clay layer (Figure 15-d) sustains this last trigger mechanism.

3.5 Storegga Slide

3.5.1 Geological setting

The Storegga Slide covers an area of 85-90,000 km^2, which is one of the world's biggest underwater slides (Figure 19) with its overall volume of 3300 km^3 and an estimated area of slide scar of 30000 km^2 (Haflidason et al. 2002-a). This complex slide has earlier been interpreted to be the product of three slide events (Bugge 1983). Recently, extensive stratigraphical and chronological studies aimed at understanding the continental margin stability and the sedimentary processes within the Storegga Slide area were carried out by the University of Bergen. A number cores (gravity and Selcore) have been collected both inside and outside the slide area for this purpose. The objective of the dating project was to verify the age of the main morphological slide structures of the Storegga Slide area. Haflidason et al. (2001, 2002-a) show that the Storegga Slide has been activated/ mobilised within the same age interval ca. 8.15 ka BP.

3.5.2 Geotechnical characterisation

In the Storegga area and despite the huge geotechnical data acquired by industry, published data are rare. Geotechnical data from one IMAGES core on the Northern flank of the Storegga Slide (Figure 19) were considered in this work. Figure 20 presents the grain size distribution, the plasticity index and the liquid limit versus depth for the core MD99-2288. In most cases, the clay content from the MD99-2288 core is greater than 40 % with a liquidity limit between 40 and 75. However, at around 19 m, the liquid limit was found equal to 35 with clay content of around 26 %. In this layer, the X-ray reveals weak lamination. According to the Andrews and Martin (2000) criteria (Table 2), sediments from this layer (around 19 mbsf) are risky regarding liquefaction. Haflidason et al. (2002-b) show that sediment at this depth (19 mbsf) corresponds to the Intra Naust reflector. In the upper margin, this

reflector has been found to be a pronounced glide plane or failure plane for the main Storegga Slide.

3.5.2.1 Gas and gas hydrate

While a well-defined bottom-simulating reflection (BSR) was identified on seismic profiles from the northern flank of the Storegga Slide (Bugge 1983; Mienert and Bryn, 1997, Mienert et al. 1998, Posewang and Mienert 1999, Bouriak et al. 2000 among others), there is no physical evidence of gas hydrates in the area. According to the NGI report N° 972521-1 and based on 14 Deepwater Gas Probe (DGP) measurements from the borehole 6404/5-GB1, they conclude that the sediment tested do not contain in-situ free gas. On the other hand and according to Kvenvolden et al. (1989), at the ODP Site 644 (Vøring plateau), gas pockets, indicating gas expansion, did form in the interval between 80 to 150 mbsf and were possibly the result of gas hydrate decomposition.

3.5.3 Results and discussion

The mechanisms that initiate the Storegga Slide in this area are not well understood. While some authors associate the failure of the Storegga Slide with excess pore pressures caused by gas-hydrate dissociation after a thermal warming since last deglaciation, other authors consider that the Storegga Slide may have been triggered by offshore earthquakes. Indeed, the Storegga area has occasionally been susceptible to high-magnitude seismicity. On the other hand, the hypothesis of the gas hydrate triggering of the Storegga Slide, is defensible. It is supported by a well-defined bottom-simulating reflection (BSR) identified on seismic profiles from the northern flank of the Storegga Slide. Another causal mechanism at the origin of the Storegga Slide was mentioned by Bryn et al. (2002). They considered that "*the precondition of the slides is closely related to the pre-glacial morphology and the glacial history, which causes variation in sedimentation rate and type"*. Indeed, the glacial – interglacial variability,

which induces a sedimentary succession consisting of fine grained marine clays, rapidly overlain by dense glacial clays generates unfavourable shear stress and excess pore pressures in the underlying marine clays. They conclude that deposition in response to glacial – interglacial variability is the main causal factor for instability. Kvalstad et al. (2002) gave an explanation of the triggering mechanism of the initial phase of the Storegga Slide, which is well identified as a series of retrogressive failures. According to Kvalstad et al. (2002) a major earthquake, toe erosion in the deep part of the slope, diapiric and water expulsion processes in the ooze layers could all have contributed to initiate the Storegga Slide.

The Analysis of the geotechnical data available from the Northern flank of the Storegga slide shows that the sediment taken at around 19 m BSF from the MD99-2288 core is probably the weak layer regarding sediment liquefaction (Figure 20). Unfortunately, neither cyclic triaxial tests nor cyclic DSS tests were carried out, in this project, in order to evaluate the sediment liquefaction potential. Additional cyclic mechanical tests from this weak layer are fundamental in evaluating the risk related to liquefaction.

3.6 Trænadjupet Slide

3.6.1 Geological setting

The Trænadjupet Slide is located on the glaciated continental margin of northern Norway (~ 68^{o}N). The slide affected an area of about 14,100 km^{2} and remobilised an up to 180 m thick sediment package comprising glacigenic sediments (~160 m) and an underlying contourite unit (~20 m). A glide plane developed in the lower part of the contourite unit during the failure (Laberg et al., 2003). This stratigraphy was correlated to geotechnical bore hole 6606/3-GB1 located at 848 m water depth about 100 km south-west of the Trænadjupet Slide scar where the failed succession was sampled (Figure 22). The drilled stratigraphy included a thin (< 1 m) veneer of a Holocene winnowing lag (see Holtedahl and Bjerkli, 1974), a ~40 m

thick unit of late Weichselian glacigenic sediments, a ~40 m thick contourite drift unit, and part of the underlying late Saalian glacigenic sediments (Laberg et al., 2003).

The late Weichselian glacigenic sediments are a homogeneous grey diamicton characterised by an average grain size distribution of 25 % clay, 45 % silt, and 30 % sand. The glacigenic sediments were transported to the shelf break mainly as a subglacial, deformable till and deposited on the upper slope in front of the Fennoscandian Ice Sheet during the late Weichselian glacial maximum (Laberg et al., 2002; Dahlgren and Vorren 2003) at a sedimentation rate of up to 65 m/ka (Laberg et al., 2003). The underlying contourite drift sediments, the Nyk Contourite Drift (Laberg et al., 2001) comprises more than 50 % clay and up to 40 % silt. The contourite sediments were deposited from an alongslope flowing ocean current on the Norwegian continental slope during the late Saalian to the late Weichselian. The maximum average sedimentation rate was up to 1.2 m/ka (Laberg et al., 2001).

3.6.2 Geotechnical characterisation

3.6.2.1 Index properties

The late Weichselian glacigenic sediments show uniform values downcore and are characterised by an average water content of ~20% and an average unit weight of about 21 kN/m^3. These sediments can be classified as inorganic clays of low to medium plasticity and they have sensitivity of about 1.5. The average water content of the contourite sediments is ~40 %, and the average total unit weight about 18 kN/m^3. Also for this unit the values are uniform downcore. On the plasticity chart, these sediments mainly plot in the inorganic clays of high plasticity part and they have sensitivity larger than 2.5. During drilling, gas bubbles and cracking were reported from 45 to 50 and 70 to 75 m depths (Laberg et al., 2003).

3.6.2.2 Triaxial tests

Undrained triaxial compression tests were preformed by the Norwegian Geotechnical Institute (1998, 2002) on samples from both the late Weichselian glacigenic sediments and the contouritic sediments. All samples were consolidated to *in situ* stress conditions prior to testing. In a plot of shear stress versus axial strain the contouritic sediments sampled at 67.5 metre first showed an increasing shear stress, up to 193.5 kPa at about 0.8 % axial strain, the yield stress of the sample (Figure 23-a). Then the shear stress decreased, the decrease is linear and the shear stress dropped to about 120 kPa at 20 % strain (Figure 23-a). Over the same strain interval, the pore pressure increases exponentially to close to 200 kPa at 20 % strain (Figure 23-b). For these sediments the triaxial compression tests showed contractant behaviour and development of shear bands (Laberg et al., 2003). A similar shear stress and pore pressure behaviour was also found for the other samples of contouritic sediments tested (NGI, 2002).

When tested in the triaxial cell the glacigenic sediments showed a different behaviour. The shear stress increased to reach its maximum value (the yield stress) at 8.3 % axial strain, an order of magnitude higher strain value compared to the contouritic sediments. The yield stress was 157.7 kPa (Figure 24). With increasing strain the shear stress showed a slowly dropping trend (Figure 24). Also the pore pressure behaved differently, it increased up to about 3.5 % axial strain to reach 80 kPa, then it fell to about 40 kPa at 20 % axial strain (Figure 24). These showed a dilatant behaviour and no shear band development was identified (Laberg et al., 2003). Other samples from this unit showed a similar behaviour (NGI, 1998).

3.6.3 Results and discussion

Undrained instability under contractive shear conditions begins when the sediment structure yields. At yield, the sediment structure begins to break down, the compressibility of the sediment increases significantly and, consequently, the porewater pressure increases

(Terzaghi et al., 1996). Of the two types of sediments tested, the contouritic sediments show indications of instability under undrained conditions as they display decreasing shear stress, porewater pressure increase and sediment deformation through shear band development (Laberg et al., 2003). This lead us to suggest that in the area of the Trænadjupet Slide the contouritic sediments were the weak layer that initially failed.

The two most likely short-term triggers of undrained instability in the Trænadjupet Slide area are seismic loading and gas hydrate dissociation (see Table 1). However, from this area no cyclic triaxial tests to identify the build up of pore pressure generated within the contouritic sediments during an earthquake as a function of loading amplitude have been conducted, and gas hydrate bearing sediments have so far not been identified in this area. The only slope stability assessment of this area is based on the Finite Element modelling by Leynaud and Mienert (2003). They found that the slide triggering impacted preferably the upper 40 metres of the sediment column. The trigger could have been caused by one large earthquake of magnitude larger than M_S 5.8, initiating retrogressive failure but cyclic loading due to several earthquakes could also explain the slide, affecting the shearing resistance in the contourite sediments by excess pore pressure generation. A similar conclusion, i.e. excess pore pressure generation by earthquakes was reached by Laberg and Vorren (2000) who also pointed out that rapid accumulation of the glacigenic sediments, the low permeability of these sediments and possibly gas charging were causal factors contributing to the slope instability in this area.

4 CONCLUSION

In this work, we have analysed the different slope failures events from the Costa target areas, which reflect diverse triggering mechanisms. Among the three external mechanisms studied to identify the geotechnical response of the sediment and to evaluate the consequence on the slope stability (earthquakes, rapid sediment accumulation and gas hydrate melting), we can mention that the excess pore pressure was recognized as a key parameter for the assessment of

slope stability. Laboratory tests can be considered as an alternative to in-situ measurement for the mechanical behaviour of the sediment, but cannot substitute the monitoring of the excess pore pressure. In this project, only one site in the Adriatic Sea was monitored in order to identify the relation between earthquake and excess pore pressure. Unfortunately, the long term pore pressure monitoring failed.

The geotechnical properties of the sediment from six different Costa areas were presented and discussed in order to identify or at least improve our understanding of the origin of the different observed slides. In the following, we present the main conclusions concerning the observed slides from the different Costa areas:

Adriatic Shelf:

The two most likely short-term triggers of undrained instability in the Adriatic Shelf area are seismic loading and rapid accumulation. The excess pore pressure generated by the sedimentation accumulation during the last 5.5 ka was evaluated and it corresponds to 6% of the hydrostatic pressure at the level of the maximum flooding surface (mfs). This excess pore pressure is low to be considered alone as a causal mechanism for the observed mud reliefs.

The four cyclic tests carried out on samples from the Adriatic slope show that sediment from the basal unit is more susceptible to liquefaction than the surrounding sediments. However, additional triaxial cyclic tests on samples from the basal unit must be carried out in order to be certain of this feature of behaviour.

Afen: Based on seismic, sedimentological and palaeooceanographic data the Afen Slide is interpreted to have failed along a surface at least partly made up of contouritic sands. Apart from being inherently less coherent than clayey sediments, sandier sediments are also susceptible to liquefaction under dynamic loading. Rapidly creating not only a localised plane of weakness but also the potential for raising the pore pressure of the surrounding cohesive sediments. It is impossible to be certain in this case whether it was the short-term liquefaction

of the sands or the secondary process of weakening the surrounding clayey sediments that provided the plane of weakness along which the slide did eventually fail. This hypothesis is strengthened by the presence of a palaeo slide almost coincident with the Afen Slide, both lie close to the Victory Transfer Zone providing the focus for seismic activity. This combined with the absence of other causative factors such as oversteepening, rapid sedimentation or gas-hydrates make a seismogenic trigger the most likely explanation.

Big'95: Data obtained from BIG'95 cores allow inferring that the location of the channel-levee deposits was probably an important factor controlling the location and morphology of the failure scar, and triggering of the debris flow (Urgeles et al., 2003). This is supported by the fact that under-consolidation seems to be present in core CLKS02 on the flank of a levee, and it is believed that the higher sedimentation rates within this system result in higher pore pressures and lower shear strengths. Local uplift and oversteepening due to volcanic activity, as shown by seismic reflection profiling and morphology derived from the multibeam echosounder (Lastras et al., 2002) are also important causal factors to be considered.

Nice slope: In this area, the liquefaction risk generated by an earthquake is low due to lack of loose sediments. The 1979 accident was generated after an exceptionally heavy rainfall and river discharge. This last observation reinforces the hypothesis of rapid accumulation or seepage of fresh water as a distinct or simultaneous possible trigger mechanisms at the origin of the Nice slope failure. On the other hand, the good concord between the maximum thickness of the failure surface (at around 50 mbsf - Figure 13-b) below the harbour extension and the depth of the very sensitive clay layer (Figure 15-d) supports the human activity as a trigger mechanism of the Nice slope.

Storegga Slide: The trigger mechanisms that initiated the Storegga Slide are not well understood. For Kvalstad et al. (2002) a major earthquake, toe erosion in the deep part of the slope, diapiric and water expulsion processes in the ooze layers could all have contributed to

initiate the Storegga Slide. On the other hand, while a BSR was identified by several authors on seismic profiles from the northern flank of the Storegga Slide, the sediment tested from two boreholes in the same area (NGI report 972521-1) does not show free gas.

The Analysis of the geotechnical data available from the Northern flank shows that the sediment taken at around 19 m BSF from the MD99-2288 core is probably the weak layer regarding sediment liquefaction.

Trænadjupet Slide: The two most likely short-term triggers of undrained instability in the Trænadjupet Slide area are seismic loading and gas hydrate dissociation. However, gas hydrate bearing sediments have so far not been identified in this area. The trigger could have been caused by one large earthquake but cyclic loading due to several earthquakes could also explain the slide, affecting the shearing resistance in the contourite sediments by excess pore pressure generation. Rapid accumulation of the glacigenic sediments, the low permeability of these sediments and possibly gas charging may be considered as causal factors contributing to the slope instability in this area.

Acknowledgements. This work has been developed within the European project COSTA (EVK3-1999-00028). *Authors have benifited from the support of the EC funded projects EURODOM (RTN2-2001-00281), EUROSTRATAFORM (EVK3-2001-00200), EURODELTA (EVK3-2001-00033) and AMASON (EVK3-2001-00067). Miquel Canals and Roger Urgeles want to express their acknowledgement to WEST-MED (REN2002-11216-E MAR / 01-LEC-EMA22F) and SPACOMA (REN2002-11217-E MAR / 01-LEC-EMA14F) projects of the ESF Euromargins initiative, to the Spanish RTD PRODELTA project (REN2002-02323), and to Generalitat de Catalunya for funding the "Barcelona Consortium on Marine Geosciences" Thematic Network (2003XT 00078) and CRG on Marine Geosciences (1999SGR-00063). Roger Urgeles contribution to the present paper has been made as part of a "Ramon y Cajal" contract.* An insightful review of Farrokh Nadim and an anonymous reviewer helped to

improve an earlier version of the manuscript. This is ISMAR CNR-Bologna contribution n. 1402.

REFERENCES.

Andrews, D. C. A., Martin, G. R., 2000. Criteria for Liquefaction of Silty Soils. 12th World Conference on Earthquake Engineering, Proceedings, Auckland, New Zealand.

Bouriak, S., Vanneste, M., Saoutkine, A., 2000. Inferred gas hydrates and clay diapirs near the Storegga Slide on the southern edge of the Vøring Plateau, offshore Norway. Marine Geology 163, Issues 1-4, 125-148.

Bourillet, J.-F., C., Edy, and A., Normand. 1992. Nouvel ensemble pour la reconnaissance du plateau continental: Sondeur multifaisceaux EM1000 et logiciel Trismus. Un exemple : la Baie des Anges (France). CIESM, Rapp. Comm. int. Mer Médit.. Monaco 33: 112.

Bryn, P., Berg, K., Lien, R., Solheim, A., Ottesen, D., Rise, L. 2002. The Storegga geomodel and its use in slide risk evaluation: geological and geotechnical site investigations in the Storegga Slide area. Proc. Offshore Site Investigation and Geotechnics: diversity and sustainability, London, UK, pp. 219-232.

Bugge, T., 1983. Submarine slides on the Norwegian continental margin, with special emphasis on the Storegga area. Continental Shelf and Petroleum Research Institute (IKU) Publication 110, Trondheim, Norway.

Campanella, R G., Gillespie, D., and Robertson, P. K., 1982. Pore pressures during cone penetration testing, *Proceedings of the 2nd European Symposium on Penetration Testing,* ESOPT-2, Amsterdam, Vol. 2, pp 507 - 512.

Canals, M., Casamor, J.L., Urgeles, R., Lastras, G., Calafat, A.M., De Batist, M., Masson, D.G., Berné, S., Alonso, B., Hughes Clarke, J.E., 2000. The Ebro Continental margin, Western Mediterranean Sea: Interplay between canyon-channel systems and mast wasting processes. GCSSEPM Foundation, 20th Annual Research Conference, Houston, Texas.

Cartwright, J.A., 1994. Episodic basin-wide hydrofracturing of overpressured Early Cenozoic mudrock sequences in the North Sea Basin. Marine and Petroleum Geology 11, 587-607.

Cattaneo A., et al., this volume. Morphobathymetric analysis of seafloor undulations on the Adriatic shelf and comparison to known examples of deepwater sediment waves. Marine Geology (this volume).

Cattaneo, A., Correggiari, A., Langone, L., Trincardi, F., 2003a. The late-Holocene Gargano subaqueous delta, Adriatic shelf: Sediment pathways and supply fluctuations. Marine Geology 193, 61-91.

Cattaneo, A., Correggiari, A., Penitenti, D., Trincardi, F., Marsset, T., 2003b. Morphobathymetry of small-scale mud reliefs on the Adriatic shelf. In: Locat, J., Mienert, J. (Eds.) Submarine Mass Movements and Their Consequences. Kluwer Academic Publisher, Amsterdam, 389-396.

Correggiari, A., Trincardi, F., Langone, L., Roveri, M., 2001. Styles of failure in heavily-sedimented highstand prodelta wedges on the Adriatic shelf. Journal of Sedimentary Research 71, 218-236.

Cochonat, P., Bourillet, J.-F., Savoye, B., Dodd, L., 1993. Geotechnical Characteristics and Instability of Submarine Slope Sediments, the Nice Slope (N-W Mediterranean Sea). Marine Georesources and Geotechnology 11: 131-151.

Clavell, E., Berastegui, X., 1991. Petroleum geology of the Gulf of València. In: A.M. Spencer (Ed.), Generation, accumulation, and production of Europe's hydrocarbons, Sp. Publ. European Association of Petroleum Geoscientists, Oxford University Press, 1: 355-368.

Cochonat, P., J.-F., Bourillet, B., Savoye. 1993. Geotechnical characteristics and instability of submarine slope sediments, the Nice slope (N-W Mediterranean sea). Marine Georesources and Geotechnology 11: 131-151.

Díaz del Río, V., Rey, J. and Vegas, R., 1986. The Gulf of Valencia continental shelf: Extensional tectonics in Neogene and Quaternary sediments. Marine Geology 73: 169-179.

Dahlgren, K.I.T., Vorren, T.O., 2003. Sedimentary environment and glacial history during the last 40 ka of the Vøring continental margin, mid-Norway. Marine Geology 193, 93-127.

Dubar, M., Anthony, E.J., 1995. Holocene Environmental Change and River-Mouth Sedimentation in the Baie des Anges, French Riviera. Quaternary Research 43(3): 329-343.

Flavigny E., Desrues J., Palayer B., 1990. Le Sable d'Hostun "RF" - note technique, Revue Française de Géotechnique 53, 67-69.

Handa,Y.P., 1989. Effect of Hydrostatic Pressure and Salinity on the Stability of Gas Hydrates. J. Phys. Chem. 94, 2652-2657.

Henriet, J.-P., De Batist, M., Verschuren, J., 1991. Early fracturing of Palaeogene clays, southernmost North Sea: relevance to mechanisms of primary hydrocarbon migration. Special publication of the European Association of Petroleum Geoscientist 1, 217-227.

Haflidason, H., Sejrup, H. P., Bryn, P., Lien, P., 2001. The Storegga Slide; Chronology and Flow Mechanism, EUG XI Abstracts, pp. 740.

Haflidason, H., Sejrup, H.P., Bryn, P., Lien, R, Masson, D., Jacobs, C., Huehnerbach, V. Berg, K., 2002. The architecture and slide mechanism of the Storegga Slide, Mid Norwegian margin. The Norwegian Petroleum Society, Annual Meeting in Trondheim October 2002.NGF Abstracts and Proceedings No. 2, pp. 80-81.

Haflidason, H., Sejrup, H.P., Berstad, I.M., Nygard, A., Richter, T., Bryn, P. Lien, R. and Berg, K. 2002-b. A weak layer feature on the Northern Storegga Slide escarpment. In: Mienert, J. and Weaver, P.P.E. (eds) European Margin Sediment Dynamics, Springer, Berlin, 37-43.

Hobbs, P.R.N., Long, D., Northmore, K.J., 1997. Modelling slope stability conditions on the West Shetland Slope. British Geological Survey Technical Report WN/97/32C.

Holtedahl, H., Bjerkli, K., 1974. Pleistocene and Recent sediments of the Norwegian continental shelf (62°N-71°N), and the Norwegian Channel area. Norges Geologiske Undersøkelse 316, 241-252.

Ishihara, K.,1985. Stability Of Natural Deposits During Earthquakes. 11th International Conference on Soil Mechanics and Foundation Engineering, Proceedings, San Francisco, v. 1, pp 321-376.

Kvalstad, T.J., Gauer, P., Kaynia, A.M., Nadim, F., 2002. Slope stability at Ormen Lange. Proc. Offshore Site Investigation and Geotechnics: diversity and sustainability, London, UK, pp. 233-250.

Kvenvolden KA, Golan-Bac M, McDonald TJ, Pftaum RC, and Brooks JM (1989) Hydrocarbon gases in sediment of the Vøring plateau, Norwegian Sea. In: Eldholm O, Thiede J, and Taylor E (Ed) Proceedings of the Ocean Drilling Program, Scientificc Results 104 : 319-326

Keefer, D.K., 1984. Landslides caused by earthquakes. Bulletin of the Geological Society of America 95, 406-421.

Laberg, J.S., Vorren, T.O., 2000. The Trænadjupet Slide, offshore Norway - morphology, evacuation and triggering mechanisms. Marine Geology 171, 95-114.

Laberg, J.S., Dahlgren, K.I.T., Vorren, T.O., Haflidason, H., Bryn, P., 2001. Seismic analyses of Cenozoic contourite drift development in the Northern Norwegian Sea. Marine Geophysical Researches 22, 401-416.

Laberg, J.S, Vorren, T.O., Mienert, J., Evans, D., Lindberg, B., Ottesen, D., Kenyon, N.H., Henriksen, S., 2002. Late Quaternary paleoenvironment and chronology in the Trænadjupet Slide area offshore Norway. Marine Geology 188, 35-60.

Laberg, J.S., Vorren, T.O., Mienert, J., Haflidason, H., Bryn, P., Lien, R., 2003. Preconditions leading to the Holocene Trænadjupet Slide offshore Norway. In: Advances in natural and technological hazards research (Locat ,J. and Mienert, J. Eds.), Kluwer, Dordrecht, The Netherlands, 247-254.

Lastras, G., Canals, M., Hughes-Clarke, J.E., Moreno, A., De Batist, M., Masson, D.G. and Cochonat, P., 2002. Seafloor imagery from the BIG'95 debris flow, western Mediterranean. Geology 30, 871-874.

Lastras, G., Canals, M., and Urgeles, R., 2003. Lessons from sea-floor and subsea-floor imagery of the BIG'95 scar and deposit, In: Advances in natural and technological hazards research (Locat ,J. and Mienert, J. Eds.), Kluwer, Dordrecht, The Netherlands, 425-432.

Leynaud, D., Mienert, J., 2003. Slope stability assessment of the Trænadjupet Slide area offshore the Mid-Norwegian margin. In: Advances in natural and technological hazards research (Locat ,J. and Mienert, J. Eds.), Kluwer, Dordrecht, The Netherlands, 255-266.

Liu A.H., Stewart J.P., Abrahamson N.A., Moriwaki Y., 2001. Journal of Geotechnical and Geoenvironmental Engineering, 127, Issue 12, 1017-1026.

Locat J., Lee H.J., 2002. Submarine landslides: Advances and challenges, Canadian Geotechnical Journal 39, Issue 1, 193-212.

Long, D., Stevenson, A.G., Wilson, C.K., Bulat, J. 2003. Slope failures in the Faroe - Shetland Channel. In: Advances in natural and technological hazards research (Locat ,J. and Mienert, J. Eds.), Kluwer, Dordrecht, The Netherlands, 281-290.

L'homer, A., 1980. Quaternaire-Précontinent et littoraux. In: S. Debrand-Passard (Editor), Synthèse géologique du sud-est de la France. Mémoire BRGM, pp. 559-561.

Maillard, A., Mauffret, A., Watts, A.B., Torné, M., Pascal, G., Buhl, P. and Pinet, B., 1992. Tertiary sedimentary history and structure of the Valencia trough (western Mediterranean). In: E. Banda and P. Santanach (Eds.), Geology and Geophysics of the Valencia Trough, Western Mediterranean. Tectonophysics 203. 57-75.

Marsset, T., Marsset, B., Thomas, Y., Cochonat, P., Cattaneo, A., Trincardi, F., 2003. Detailed anatomy of late Holocene deposits on the Adriatic shelf from 3D very high resolution seismic data (TRIAD survey). In: Advances in natural and technological hazards research (Locat ,J. and Mienert, J. Eds.), Kluwer, Dordrecht, The Netherlands, 449-458.

Trincardi F., Cattaneo A., Correggiari A., Sultan N., this volume. Seafloor irregularities, fluid escape and sediment deformation above a possible regional weak layer within late-Holocene muddy deposits (Adriatic shelf, Italy). Marine Geology (this volume).

Masson, D.G. 2001. Sedimentary processes shaping the eastern slope of the Faeroe – Shetland Channel. Continental Shelf Research 21, 825-857.

Mienert, J., Bryn P., 1997. Gas hydrate drilling conducted on the European Margin. EOS, Transactions, American Geophysical Unio, 78: 49, 567-571.

Mienert, J., Posewang, J. & Baumann, M., 1998. Gas hydrates along the north-eastern Atlantic margin: possible hydrate bound margin instabilities and possible release of methane. in Henriet, J.-P. & Mienert, J. (eds); Gas hydrates: Relevance to world margin stability and climatic change, Geological Society of London, Special Publication, 137, pp. 275-291.

Muir-Wood, R. 2000. Deglaciation seismotectonics: a principal influence on intraplate seismogenisis at high latitudes. Quaternary Science Reviews, 19, 1399-1411.

Norwegian Geotechnical Institute 1998. Møre and Vøring soil investigation 1997, Vol. I and II. Report No. 972521-1, Oslo, Norway.

Norwegian Geotechnical Institute 2002. Laboratory testing, Vema/Nyk. Geotechnical testing report. Report No. 20021026-1, Oslo, Norway.

Pestana, J.M., Biscontin, G., Nadim, F., Andersen, K., 2000. Modeling cyclic behavior of lightly overconsolidated clays in simple shear, Soil Dynamics and Earthquake Engineering, 19, 501-519.

Posewang, J., Mienert, J., 1999. The enigma of double BSRs: Indicators for changes in the hydrate stability field. Geo-Marine Letters 19, 157-163.

Ramsey, N. 2002. A calibrated model for the interpretation of cone penetration tests (CPTs) in North Sea quaternary soils. Proc. Offshore Site Investigation and Geotechnics: diversity and sustainability, London, UK, pp. 341-356

Robertson, P.K., Campanella, R.G., Gillespie, D., and Grieg, J., 1986. Use of Piezometer Cone Data, *Proceedings*, Use of In-Situ Tests in Geotechnical Engineering (In-Situ '86), GSP No. 6, American Society of Civil Engineers, New York.

Robertson, P.K., 1990. Soil Classification Using the Cone Penetration Test, *Canadian Geotechnical Journal*, Vol. 27, pp. 151-158.

Rumph, B., Reaves, C.M., Orange, V.G., Robinson, D.L. 1993. Structuring and transfer zones in the Faeroe Basin in a regional tectonic context. 999-1009 In: Petroleum Geology of NW Europe, Proceedings of the 4th Conference Vol 2, Parker, J.R. ed

Seed, H. B., Idriss, I. M., 1971. Simplified Procedure for Evaluating Soil Liquefaction Potential, Journal of the Soil Mechanics and Foundations Division, ASCE, Vol. 97, No SM9,

Seed, H. B., Tokimatsu, K., Harder, L. F., Chung, R. M., 1984. The Influence of SPT Procedures in Soil Liquefaction Resistance Evaluations, Earthquake Engineering Research Center Report No. UCB/EERC-84/15, University of California at Berkeley.

Seed, H. B., Tokimatsu, K., Harder, L. F., and Chung, R. M., 1985. Influence of SPT Procedures in soil liquefaction resistance evaluations. Journal of Geotechnical Engineering, ASCE, 111(12), 1425-1445.

Seed, R. B., Cetin, K.O., Moss, R.E.S., Kammerer, A. M., Wu, J., Pestana, J. M., Riemer, M. F., 2001. Recent Advances in Soil Liquefaction Engineering, and Seismic Site Response Evaluation Paper No I.20, University of California, Berkeley, California.

Sobkowicz, J.C., Morgenstern, N.R. 1984. The undrained equilibrium of gassy sediments. Canadian Geotechnical Journal 21, 439–448.

Sols Essais 1994. Internal report.

Stewart, I.S., Sauber, J., Rose, J., 2000. Glacio-seismotectonics: icesheets, crustal deformation and seismicity. Quaternary Science Reviews 19, 1367-1389.

Stoker, M S., Hitchen, K., Graham, C., 1993. The Geology of the Hebrides and West Shetland Shelves and adjacent deep-water areas. HMSO for the British Geological Survey.

Stoker, M S., Leslie, A B., Scott, W D., Briden, J C., Hine, N M., Harland, R., Wilkinson, I P., Evans, D., Ardus, D A.,1994. A record of late Cenozoic stratigraphy, sedimentation and climate change from the Hebrides Slope, NE Atlantic Ocean. Journal of the Geological Society of London.151, 235-249

Sultan N., Cochonat P., Bourillet J.F., Cayocca F, 2001. Evaluation of the risk of marine slope instability: A pseude-3d approach for application to large areas, Marine Georesources and Geotechnology 19, Issue 2, 107-133.

Sultan, N., Cochonat, P., Foucher, J.P., Mienert, J., this volume. Effect of gas hydrates melting on seafloor slope instability.

Terzaghi, K., Peck, R.B., Mesri, G., 1996. Soil mechanics in engineering practice. 3rd edition. John Wiley & Sons, Inc., New York.

Urgeles, R., Lastras, G., Canals, M., Willmott, V., Moreno, A., Casas, D., Baraza, J., Berné, S., 2003. The BIG'95 debris flow and adjacent unfailed sediments in the NW Mediterranean Sea: geotechnical-sedimentological properties, and dating. In: Advances in natural and technological hazards research (Locat ,J. and Mienert, J. Eds.), Kluwer, Dordrecht, The Netherlands, 479-490.

Vanoudheusden, E., Sultan, N., Cochonat, P., this volume. Mechanical behaviour of gassy sediments: experimental and theoretical approaches.

Watterson, J., Walsh, J., Nicol, A., Nell, P.A.R., Bretan P.G. 2000. Geometry and origin of a polygonal fault system. Journal of the Geological Society, London 157, 151-162.

Wilson, C.K., Long, D. and Bulat, J., 2003. The Afen Slide – a multistage slope failure in the Faroe – Shetland Channel . In: Submarine mass movements and their consequences. In: Advances in natural and technological hazards research (Locat ,J. and Mienert, J. Eds.), Kluwer, Dordrecht, The Netherlands, 317-324.

Youd, T.L., Idriss, I.M., 1997, Proceedings of the NCEER Workshop on Evaluation of Liquefaction Resistance of Soils , Technical Report NCEER-97-0022, Multidisciplinary Center for Earthquake Engineering Research, Buffalo, New York.

Figures Captions

Figure 1. Variation of median values of *N* with distance and magnitude, deep soil sites and shallow stiff soil/rock sites (with no near-fault corrections). Source: Liu et al., 2001.

Figure 2. Excess pore pressure in the simulated column for different sedimentation rates.

Figure 3. Location map of cores COS01-29 and –31 in the Adriatic Sea. Chirp sonar profiles show the position and the depth of penetration of the two cores through the basal unit of the late-Holocene mud wedge, above the maximum flooding surface (mfs). The two cores were correlated with magnetic susceptibility logs. The interval of the mfs corresponds likely to low susceptibility values.

Figure 4. Oedometer compression curves of four samples from cores COS01-29 and COS01-31.

Figure 5. Undrained cyclic triaxial test (sample A6 - σ'_{30} = 100 kPa - $\Delta q/\sigma'_{30}$ = 0.18).

Figure 6. Undrained cyclic triaxial test (sample A8 - σ'_{30} = 100 kPa - $\Delta q/\sigma'_{30}$ = 0.30).

Figure 7. a) Vertical effective stress and excess pore pressure versus depth and b) porosity versus depth evaluated from the Sedimentation Accumulation rate of core COS31.

Figure 8. Comparison of undrained shear strength between cores inside and outside the slide area (Core 122 is outside and Core 20 (HM129 20GC) is inside the debris flow)

Figure 9. High-resolution seismic section along the axis of the Afen Slide showing acoustically transparent lenses possibly contouritic sands.

Figure 10. Image from 3D data overlain with the outline of a buried landslide from 2D deep tow boomer data.

Figure 11. Bathymetry map (contour lines at 100 m interval) derived from multibeam data with outline of the BIG'95 debris flow, and location of cores discussed in this paper.

Figure 12. Schematic cross section of the Var Holocene delta, adapted from Dubar & Anthony (1995). The thick vertical lines show boreholes. See the relative position of the Nice airport and of the sediment cores.

Figure 13. a) Core locations collected during GMO1, Geosciences I and Geosciences II cruises and b) Thickness of the sediment failure determined from two sets of bathymetry data (before and after the 1979 accident). It is interesting to see that the deepest part of the slope failure is directly below the corner of the harbour extension.

Figure 14. Undrained shear strength, sensitivity and Su/σ'_v profiles from a) KGMO_03, KGMO_04, KGMO_05, KGMO_08 and b) MD01-2468G, MD01-2469G, MD01-2470 and MD01-2471.

Figure 15. Results of pz11 piezocone test (for location refer to Figure 13-a) including measurements of a) corrected cone tip resistance (qt), b) differential pore water pressure (Δu), c) sleeve friction (fs), and d) lithology profiles (see text for discussion).

Figure 16. Undrained cyclic triaxial test (S4-1 - σ'_{30} = 40 kPa - $\Delta q/\sigma'_{30}$ = 0.23)

Figure 17. Cyclic resistance ratio as a function of the cycles to liquefaction (Nice slope).

Figure 18. Analysis of the liquefaction susceptibility of the sediment layers from the Nice slope using the safety factor empirical method

Figure 19. Bathymetry of the storegga slide including drill sites and boreholes location (B 6404/5, B 6405/2 and MD992288), where geotechnical data were made available by the Industry

Figure 20. a) Grain size distribution b) plasticity index and c) Liquid limit versus depth below seabed - core MD99-2288.

Figure 21. Undrained shear strength sensitivity and Su/σ'_v profiles from MD99-2288.

Figure 22. Bathymetric map including the location of the Trænadjupet Slide and the Nyk Contourite Drift. The location of borehole 6606/3-GB1 is shown.

Figure 23. a) Shear stress versus axial strain and b) Pore pressure versus axial strain for the contouritic sediments sampled at 67.5 metre depth in borehole 6606/3-GB1.

Figure 24. a) Shear stress versus axial strain and b) Pore pressure versus axial strain for the glacigenic sediments sampled at 40.2 metre depth in borehole 6606/3-GB1.

Area	Possible Trigger Mechanisms							
	Seismic loading	Gas Hydrate dissociation	Rapid Accumulation	Gas charging	Glacial loading	Volcanic processes	Seepage	Human activities
Adriatic	□		□	□			□	
Afen	□							
Big'95	□					□		
Nice	□		□				□	□
Storegga	□	□		□	□		□	
Tranaedjupet	□	□	□					

Table 1. Possible trigger mechanisms at the origin of the observed slope failures in the COSTA working areas.

	Liquid Limit < 32	**Liquid Limit ≥ 32**
Clay Content < 10%	Susceptible	Further Studies Required
Clay Content ≥ 10 %	Further Studies Required	Not Susceptible

Table 2. Liquefaction susceptibility of silty and clayey sands (after Andrews and Martin, 2000)

MARGIN	SLIDE	WATER DEPTH (m)	LABORATORY			IN SITU	
			STATIC		CYCLIC	MEASUREMENT	MONITORING
			SATURATED SEDIMENT	*GASSY SEDIMENT*	*SATURATED SEDIMENT*		
ADRIATIC	ADRIATIC	10 - 150	■ *IGM / ifremer*		■ *IGM / ifremer*		□ IGM
EBRO	BIG 95	600	■ *UiBa*			■ *ifremer / UiBa*	
NW MED	NICE	20 - 70	■ *ifremer*		■ *ifremer*		
NORWEGIAN	STOREGGA	400 - 1200	●		●	●	
	TRÆNADJUPET	500- 2400	■ *UiT*				
UK	AFEN	830	■ *BGS*				
Synthetic Sediment				■ *ifremer*			

■ DONE, □ PLANNED; ● DATA AVAILABLE FROM INDUSTRY

Table 3. Summary of different geotechnical tests (done and planned) within the COSTA project.

SAMPLE	CORE	Depth (m BSF)	Preconsolidation pressure (kPa)	in-situ vertical effective stress (kPa)	OCR	λ
A 1	COS01-29	8.69 – 8.74	27	65	0.41	0.1879
A 2	COS01-29	8.94 – 8.99	25	67.3	0.371	0.1530
A 3	COS01-31	8.93 – 8.98	18	67.3	0.267	0.1510
A 4	COS01-31	9.40 – 9.44	19	70.32	0.27	0.1516

Table 4. Summary of the oedometer tests carried out on samples from the Adriatic slope.

SAMPLE	CORE	Depth (m BSF)	# Tests	$\Delta q/\sigma'_{30}$
A5	COS01-29	8.74-8.94	1	0.18
A6	COS01-31	8.98-9.30	1	0.18
A7	COS01-29	3.45-3.60	1	0.18
A8	COS01-29	3.60-3.75	1	0.30

Table 5. Summary of the cyclic tests carried out on samples from the Adriatic slope.

SAMPLE	CORE	Depth (m BSF)	# Tests	$\Delta q/\sigma'_{30}$
S 1	MD01-2470	7 - 7.3	2	0.24 – 0.41
S 2	MD01-2470	10 – 10.3	2	0.096 – 0.17
S 3	KGMO-04 S3	1 – 1.2	1	0.25
S 4	KGMO-05 S3 2A-3	2 - 3	5	0.096 - 0.23 - 0.50 – 0.66 - 0.83

Table 6. Summary of the cyclic tests carried out on samples from the Nice slope.

SAMPLE	% > 80 µm	Depth (m BSF)	σ'_{30} (kPa)	$\Delta q/\sigma'_{30}$
C3-1	99	37.25	100	0.4
C3-2	99	37.40	100	0.4
C4-1	70	53.30	100	1.0
C4-2	70	53.50	100	0.6
C4-3	59	53.70	200	0.5
C5-2	84	55.55	200	0.6
C8-2	64	73.00	200	0.6

Table 7. Summary of the cyclic tests carried out by Sols Essais (1994) on samples from the Nice slope.

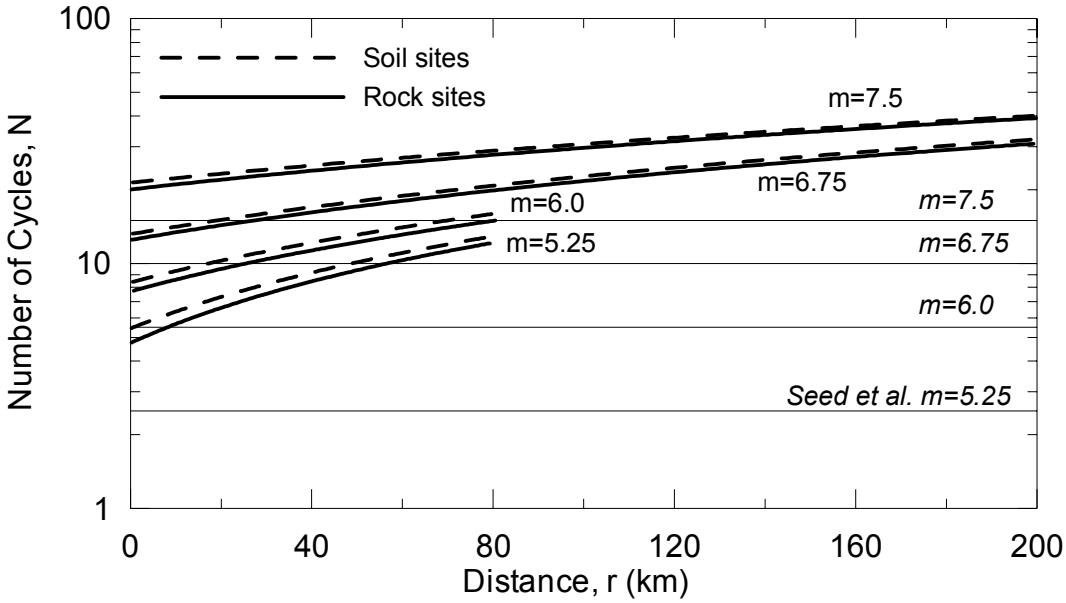

Figure 1. Variation of median values of *N* with distance and magnitude, deep soil sites and shallow stiff soil/rock sites (with no near-fault corrections). Source: Liu et al., 2001.

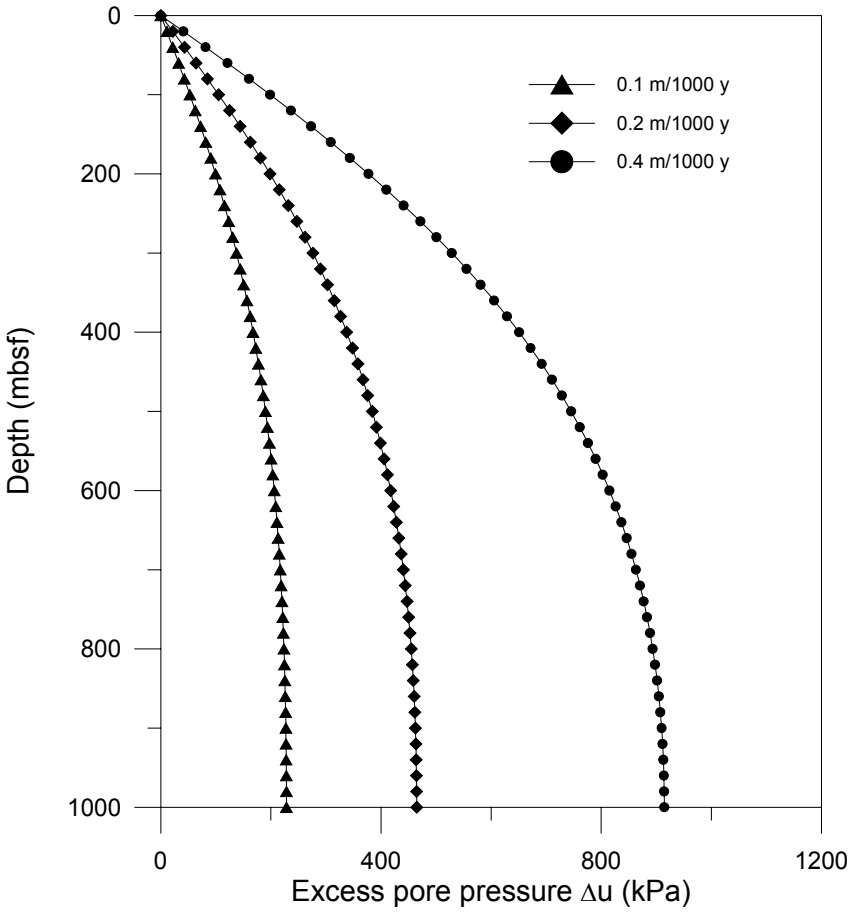

Figure 2. Excess pore pressure in the simulated column for different sedimentation rates.

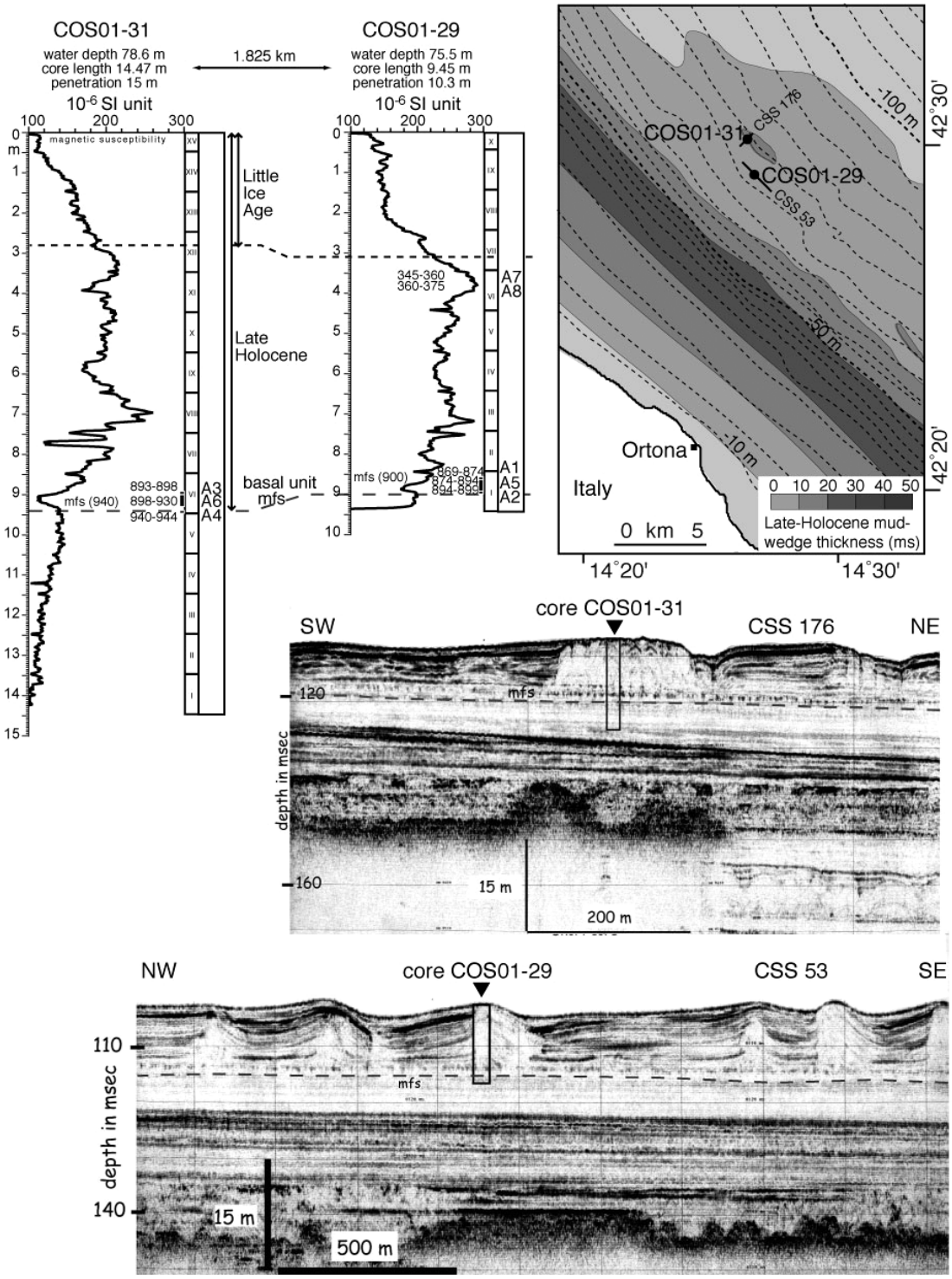

Figure 3. Location map of cores COS01-29 and –31 in the Adriatic Sea. Chirp sonar profiles show the position and the depth of penetration of the two cores through the basal unit of the late-Holocene mud wedge, above the maximum flooding surface (mfs). The two cores were correlated with magnetic susceptibility logs. The interval of the mfs corresponds likely to low susceptibility values.

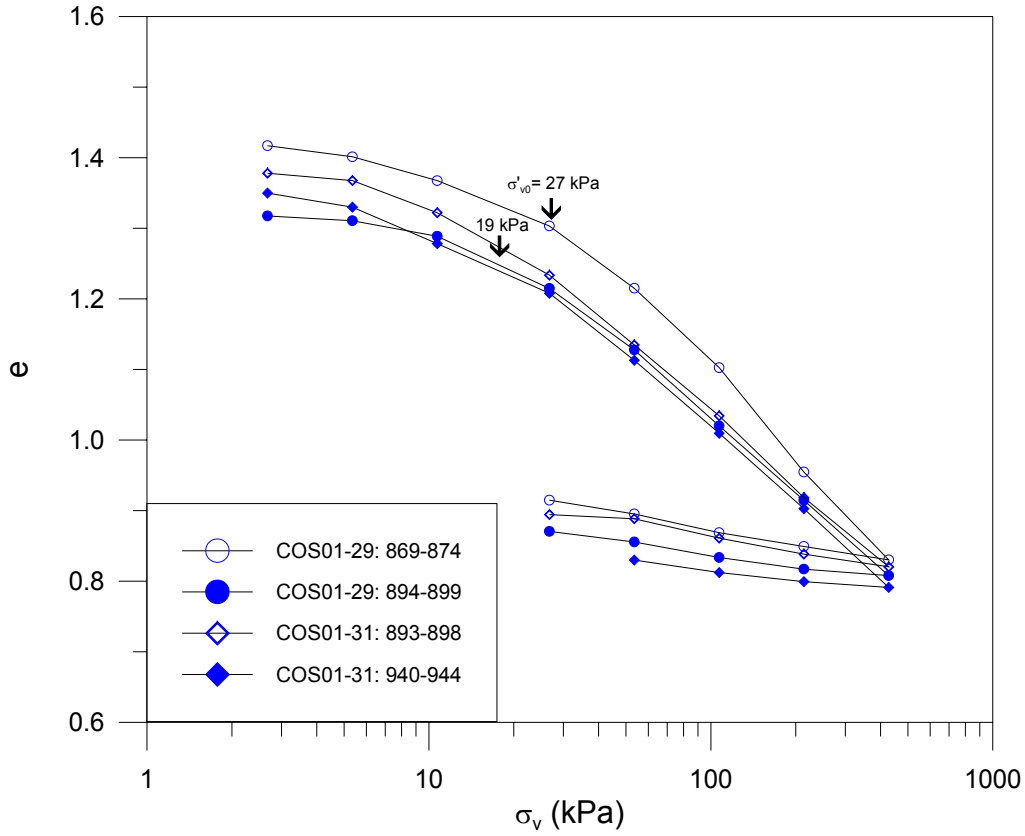

Figure 4. Oedometer compression curves of four samples from cores COS01-29 and COS01-31.

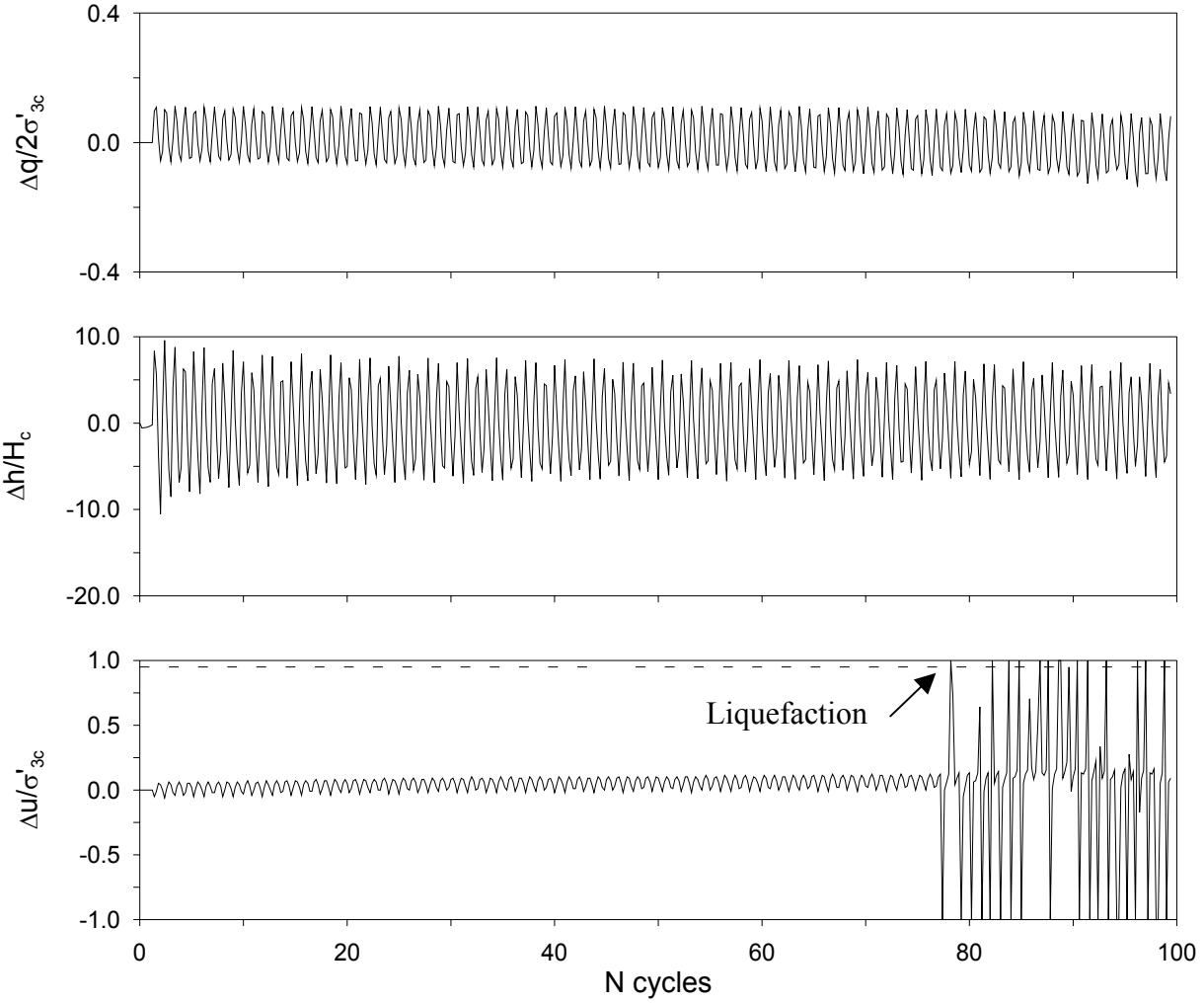

Figure 5. Undrained cyclic triaxial test (sample A6 - σ'_{30} = 100 kPa - $\Delta q/\sigma'_{30}$ = 0.18).

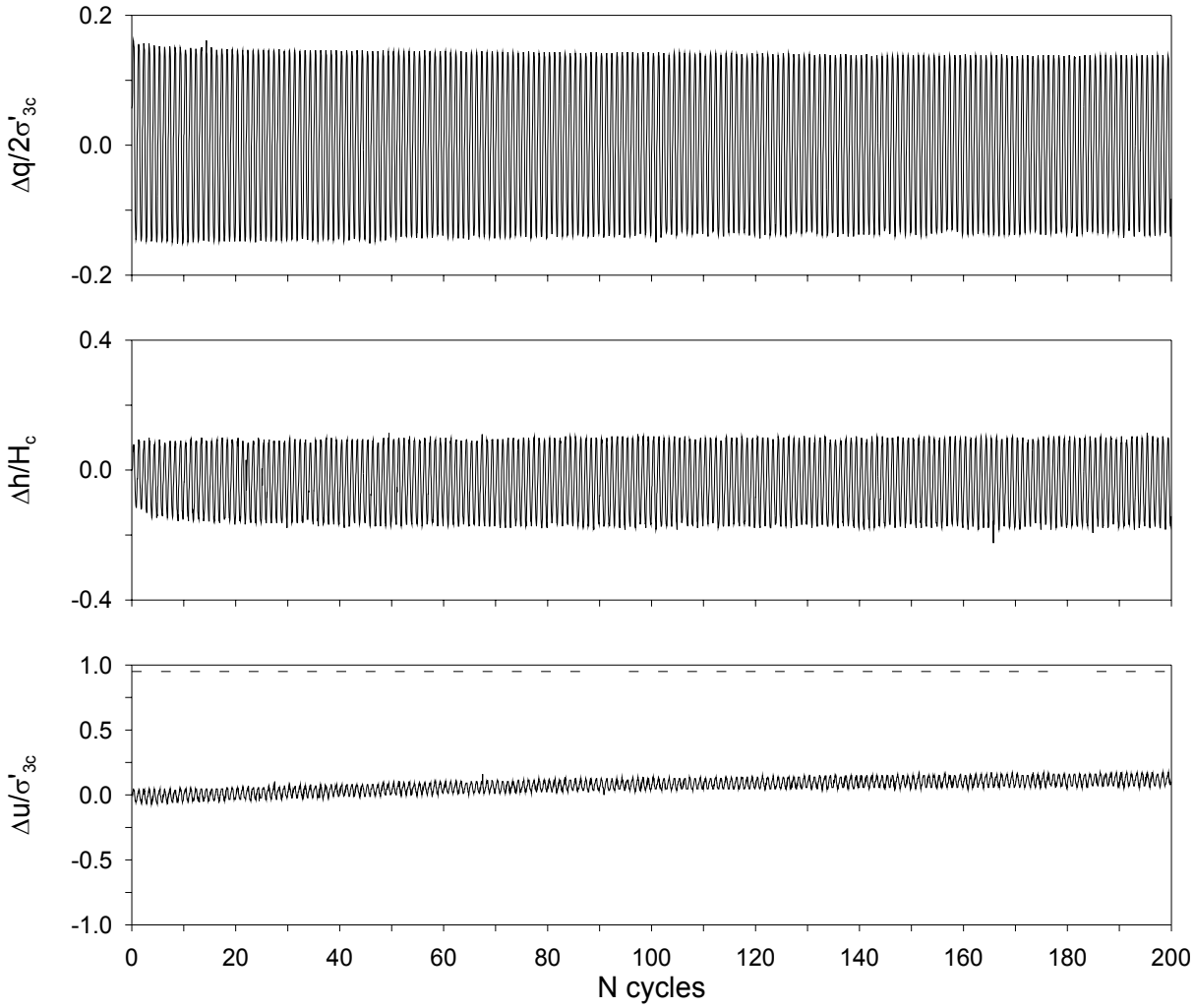

Figure 6. Undrained cyclic triaxial test (sample A8 - σ'_{30} = 100 kPa - $\Delta q/\sigma'_{30}$ = 0.30).

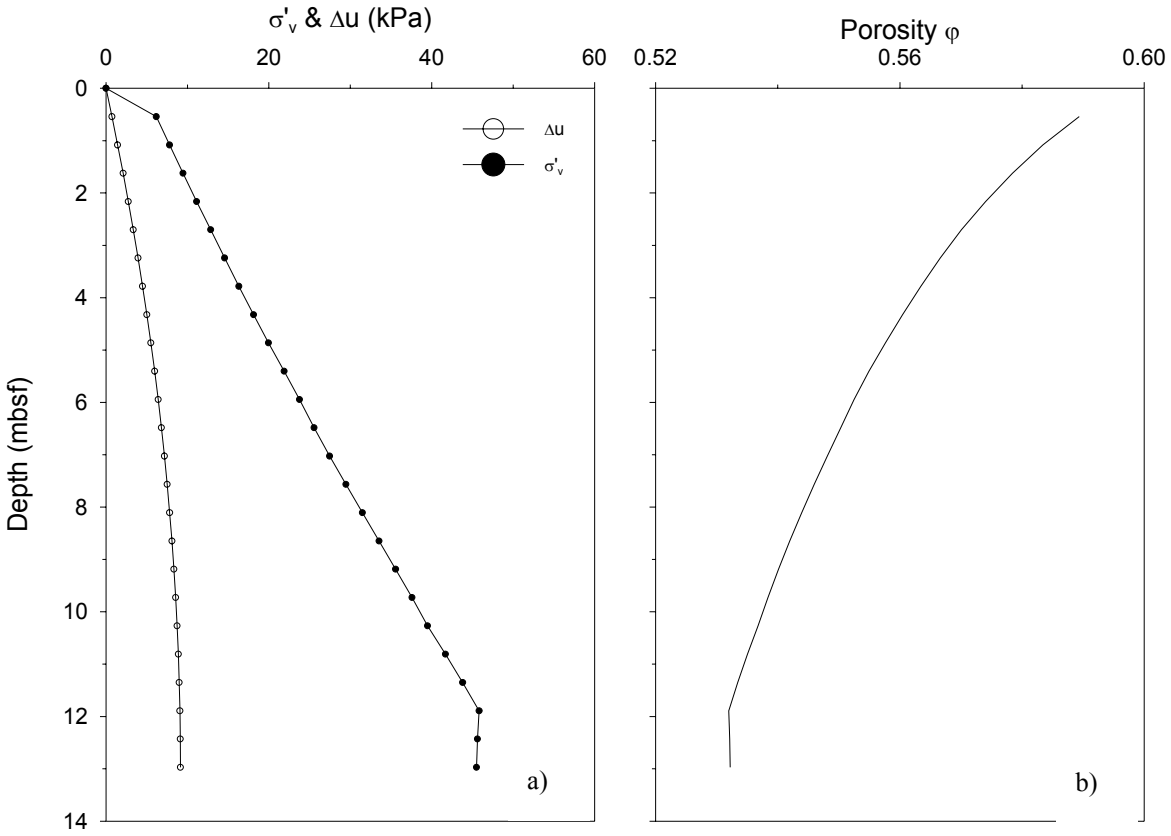

Figure 7. a) Vertical effective stress and excess pore pressure versus depth and b) porosity versus depth evaluated from the Sedimentation Accumulation rate of core COS31.

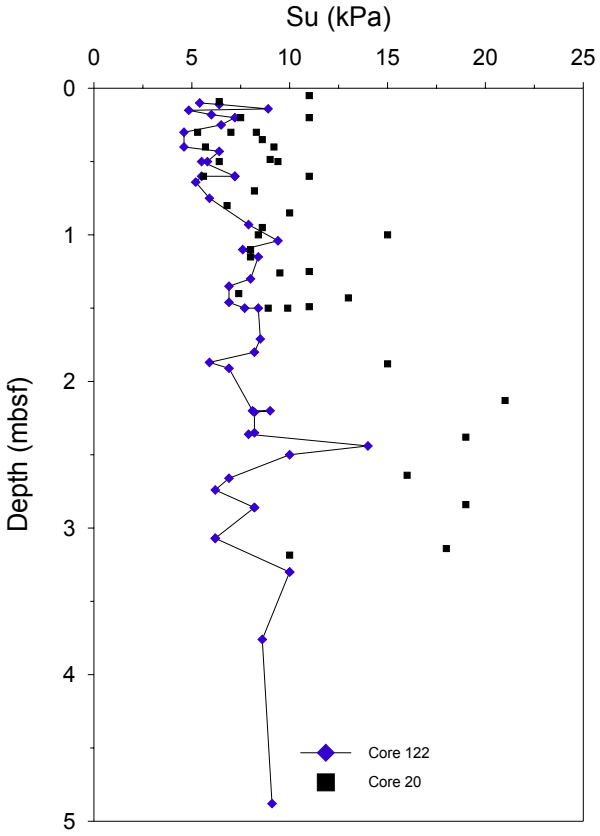

Figure 8. Comparison of undrained shear strength between cores inside and outside the slide area (Core 122 is outside and Core 20 (HM129 20GC) is inside the debris flow)

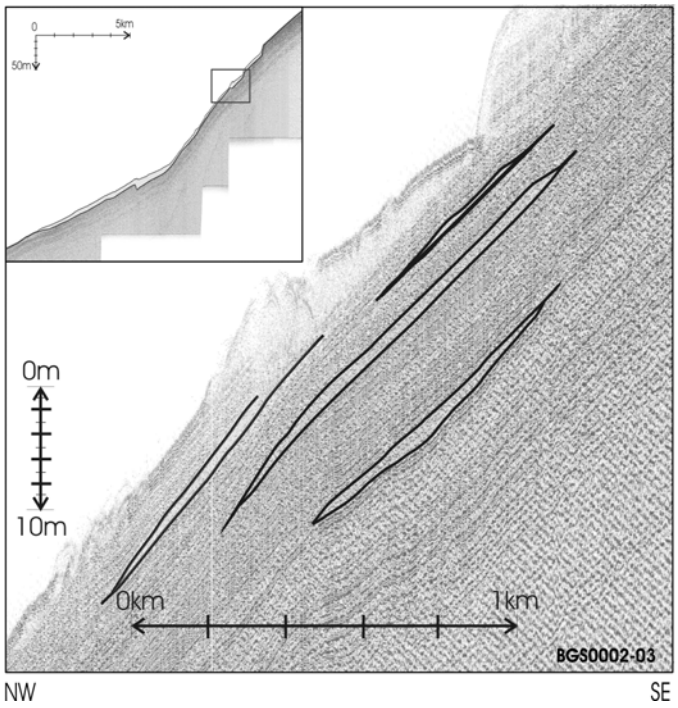

Figure 9. High-resolution seismic section along the axis of the Afen Slide showing acoustically transparent lenses possibly contouritic sands.

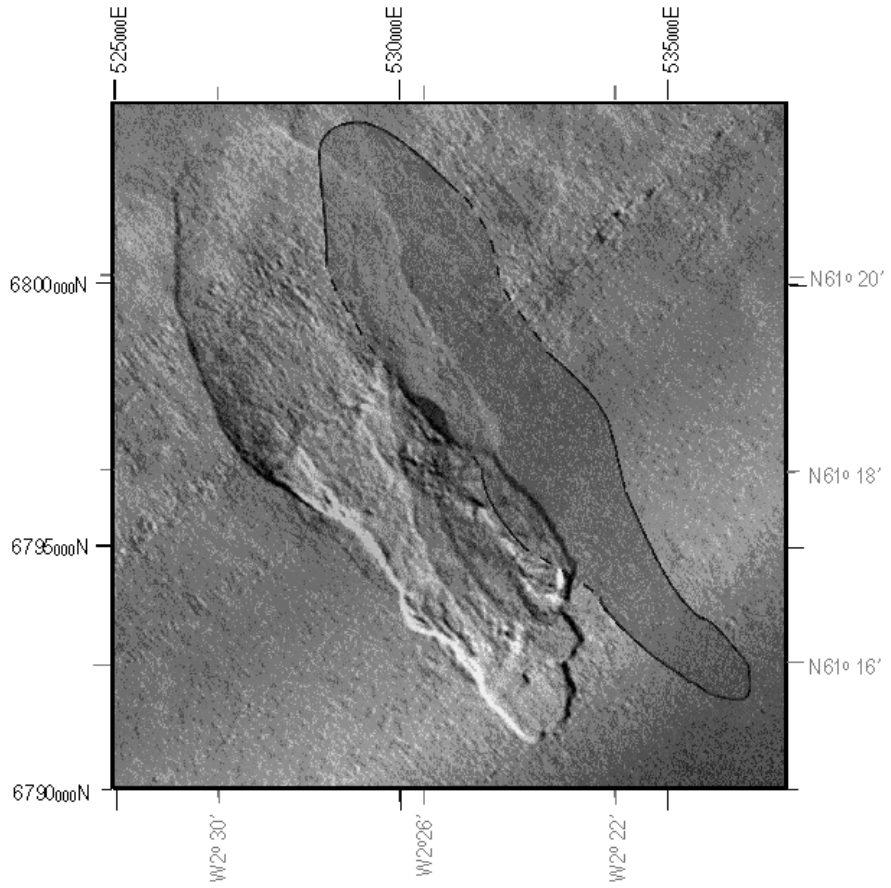

Figure 10. Image from 3D data overlain with the outline of a buried landslide from 2D deep tow boomer data.

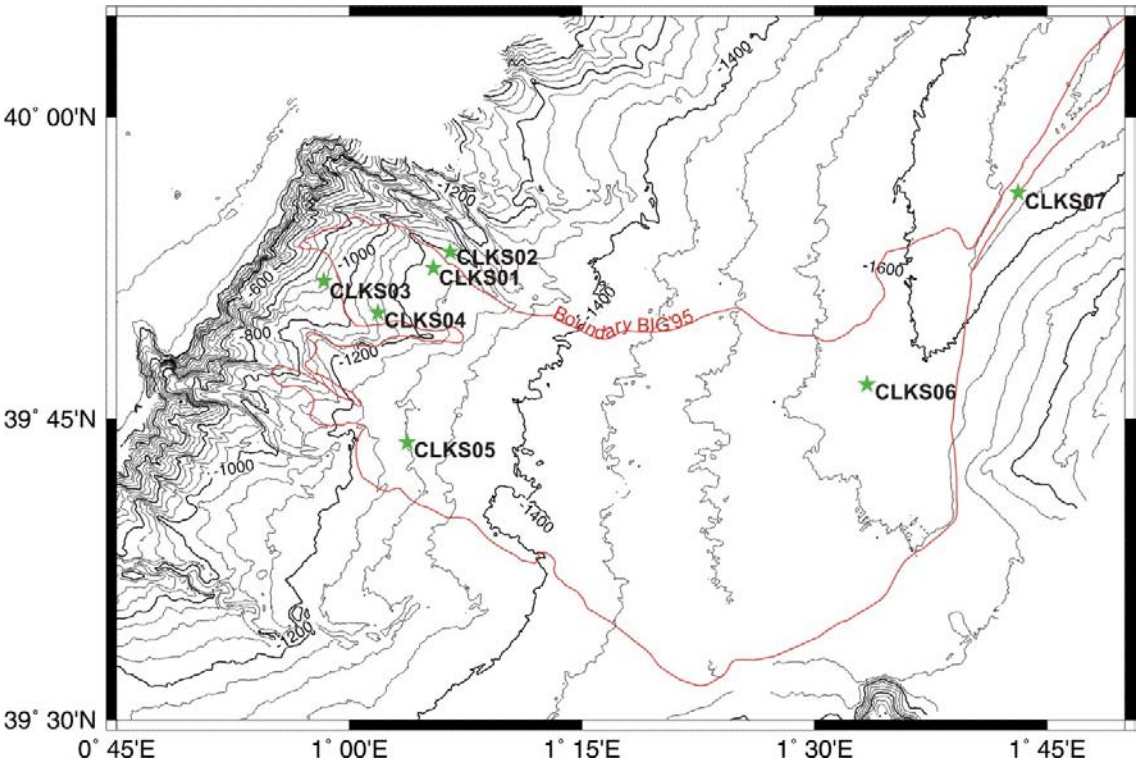

Figure 11. Bathymetry map (contour lines at 100 m interval) derived from multibeam data with outline of the BIG'95 debris flow, and location of cores discussed in this paper.

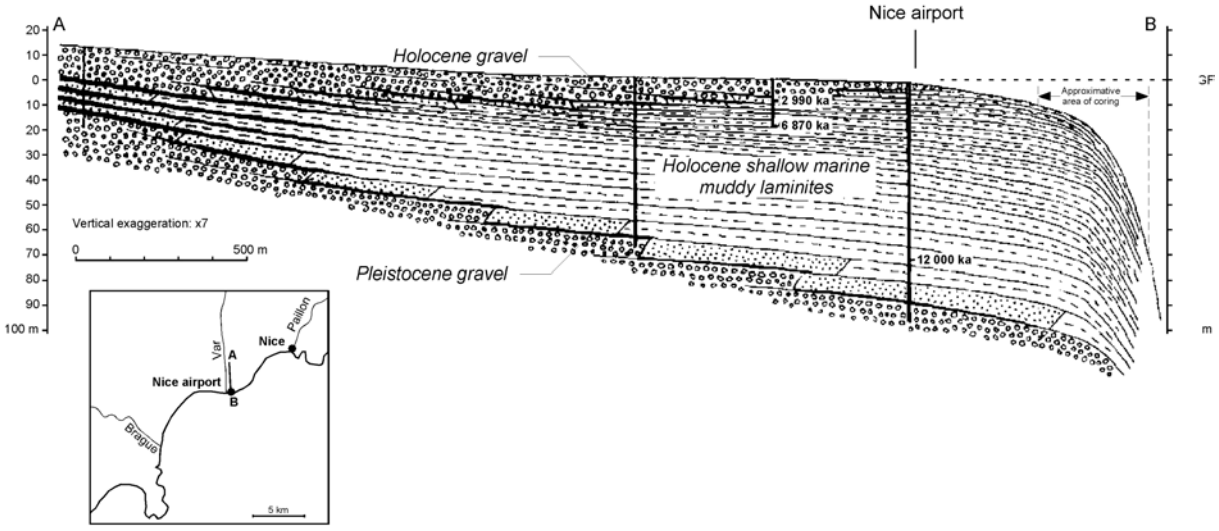

Figure 12. Schematic cross section of the Var Holocene delta, adapted from Dubar & Anthony (1995). The thick vertical lines show boreholes. See the relative position of the Nice airport and of the sediment cores.

a)

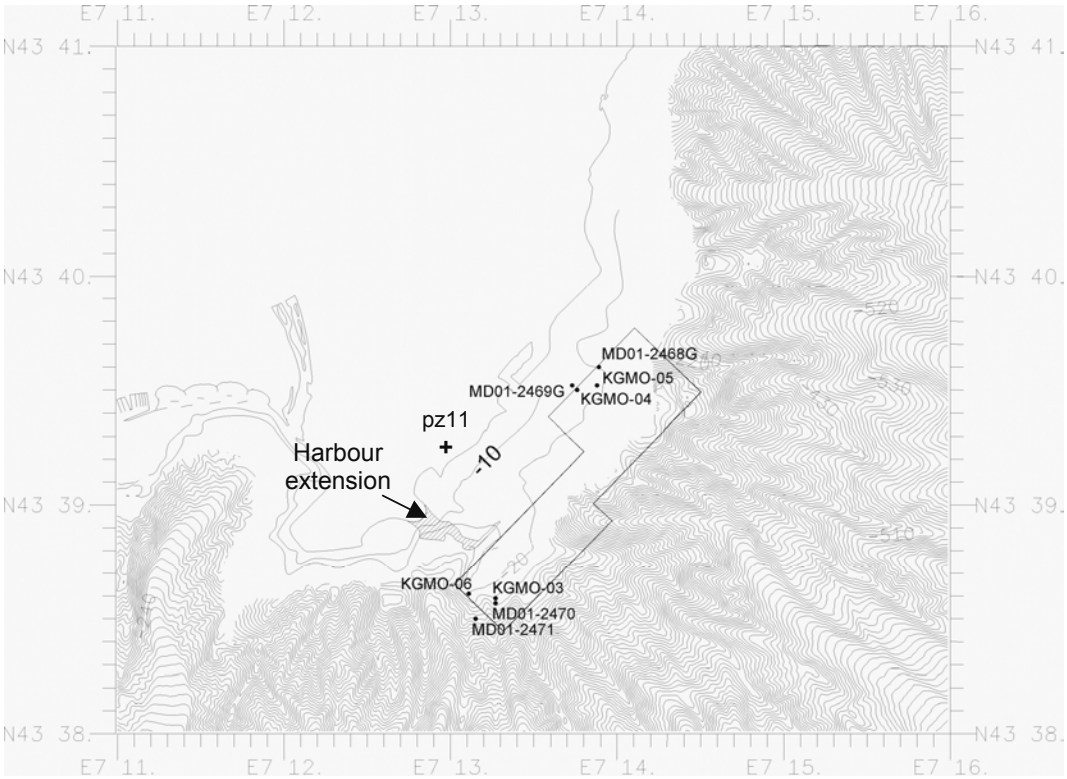

b)

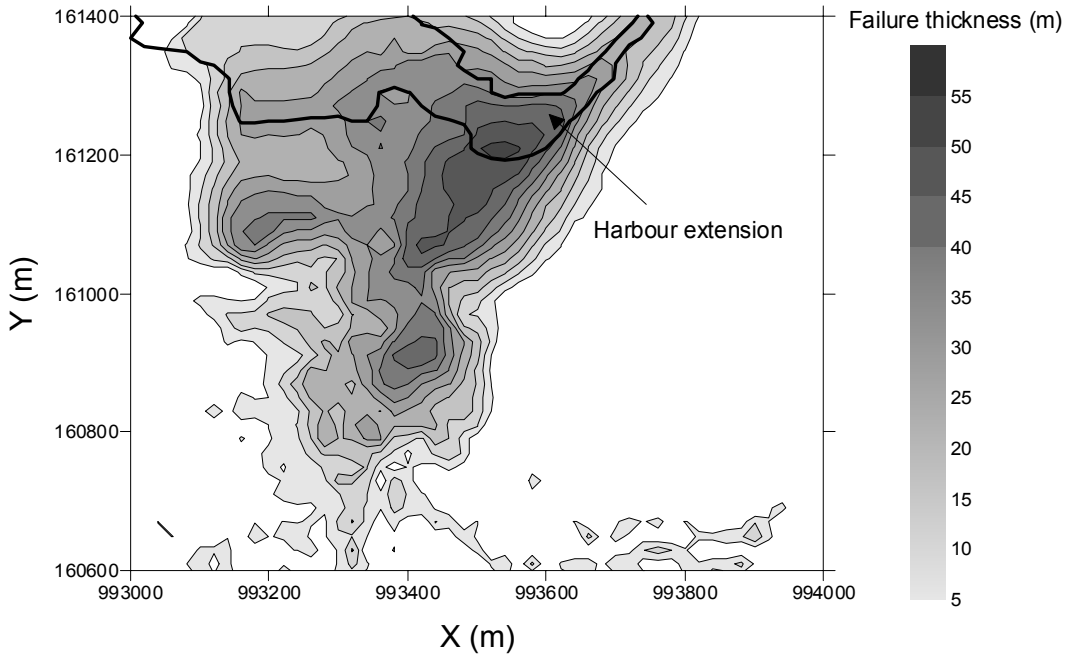

Figure 13. a) Core locations collected during GMO1, Geosciences I and Geosciences II cruises and b) Thickness of the sediment failure determined from two sets of bathymetry data (before and after the 1979 accident). It is interesting to see that the deepest part of the slope failure is directly below the corner of the harbour extension.

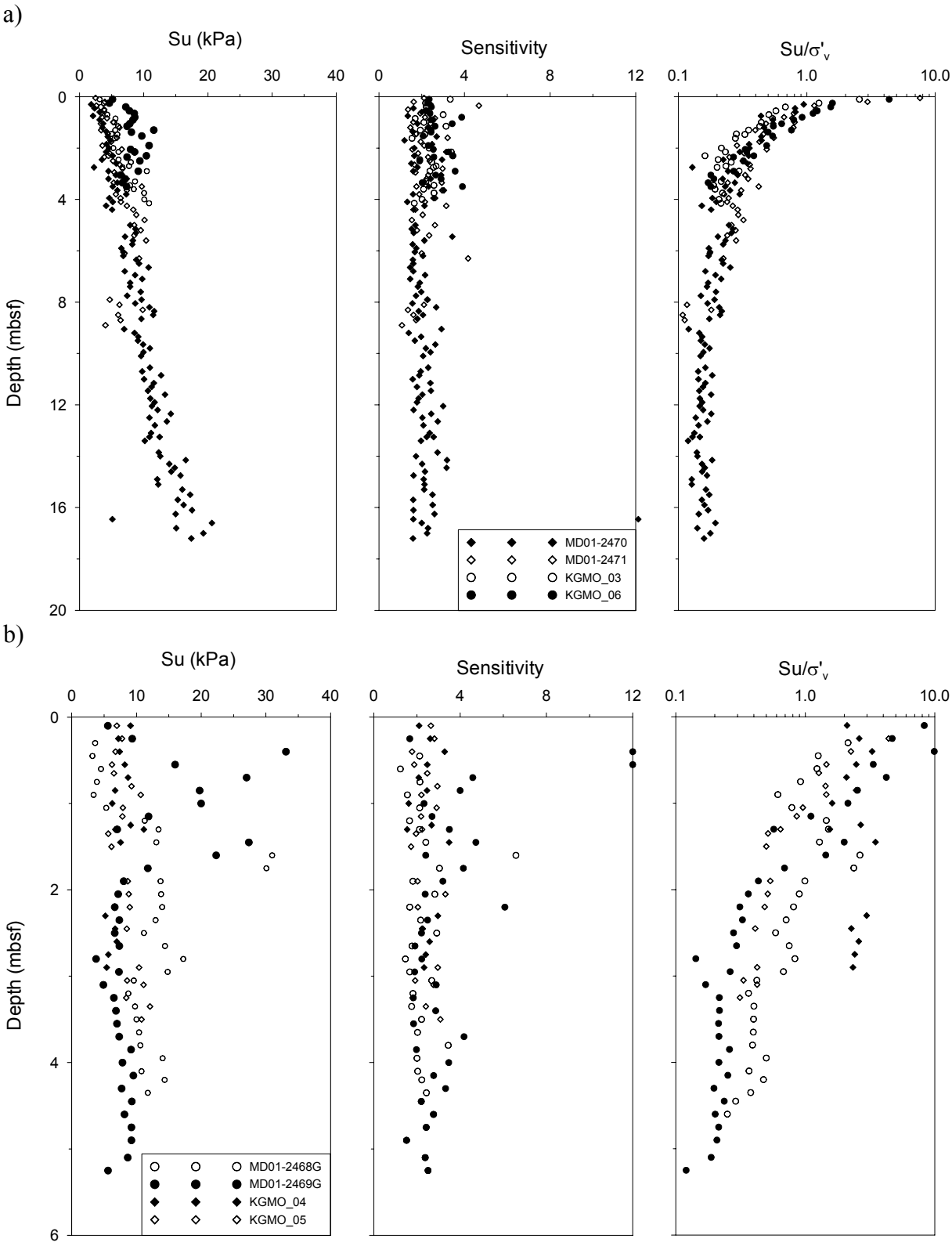

Figure 14. Undrained shear strength, sensitivity and Su/σ'$_v$ profiles from a) KGMO_03, KGMO_04, KGMO_05, KGMO_08 and b) MD01-2468G, MD01-2469G, MD01-2470 and MD01-2471.

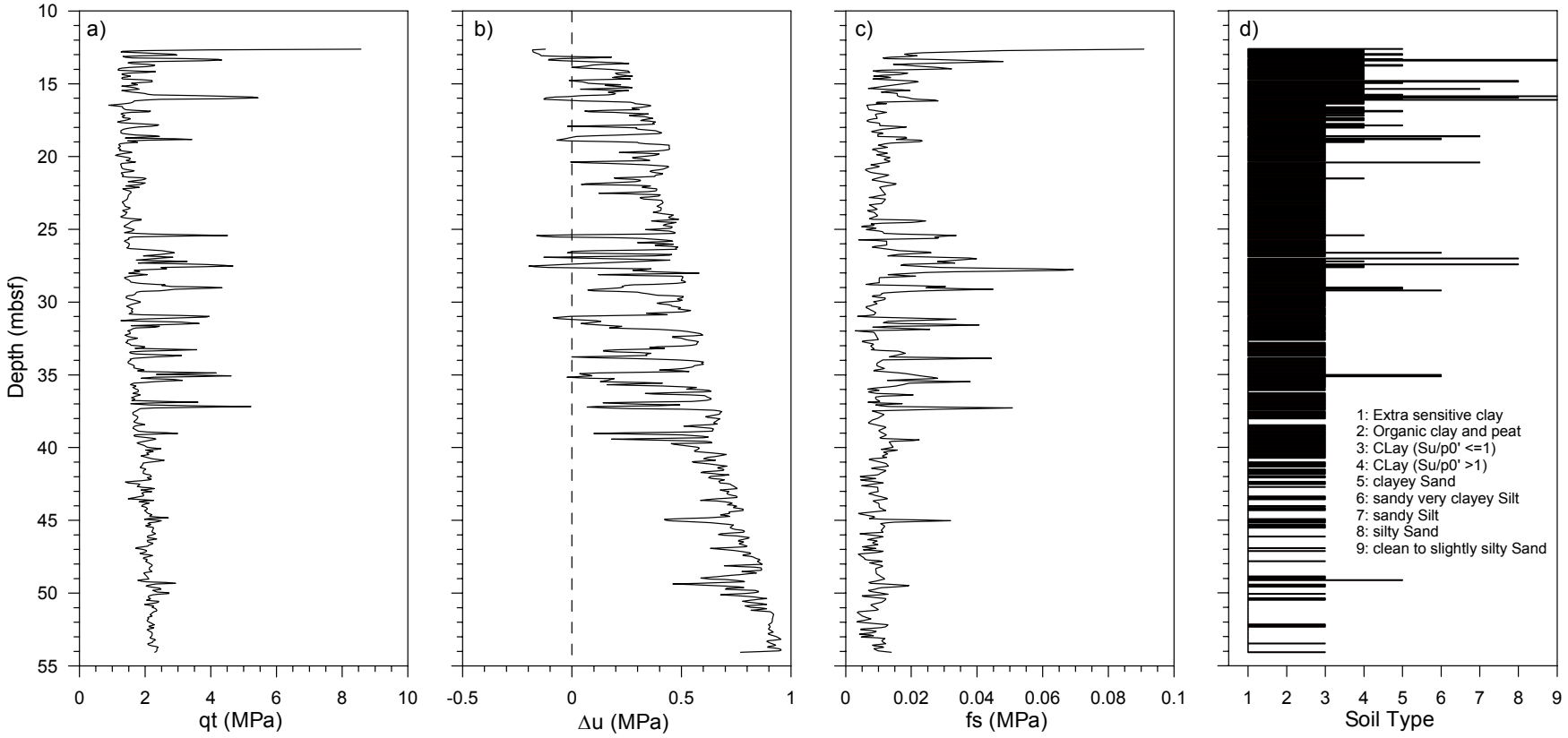

Figure 15. Results of pz11 piezocone test (for location refer to Figure 13-a) including measurements of a) corrected cone tip resistance (qt), b) differential pore water pressure (Δu), c) sleeve friction (fs), and d) lithology profiles (see text for discussion).

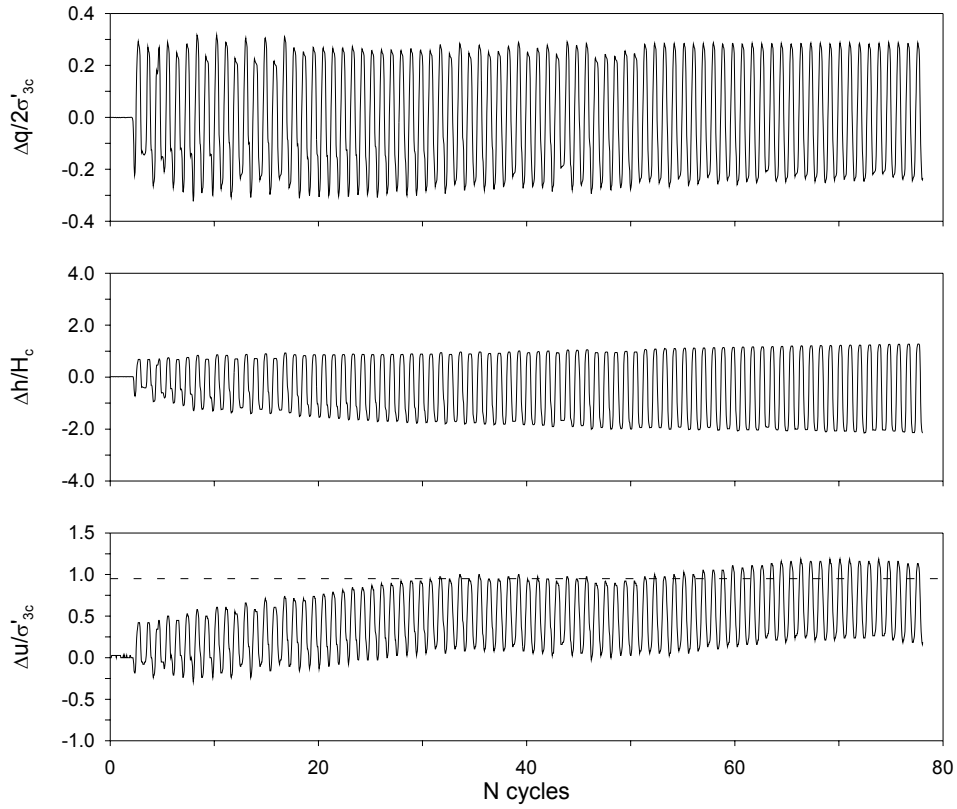

Figure 16. Undrained cyclic triaxial test (S4-1 - σ'_{30} = 40 kPa - $\Delta q/\sigma'_{30}$ = 0.23)

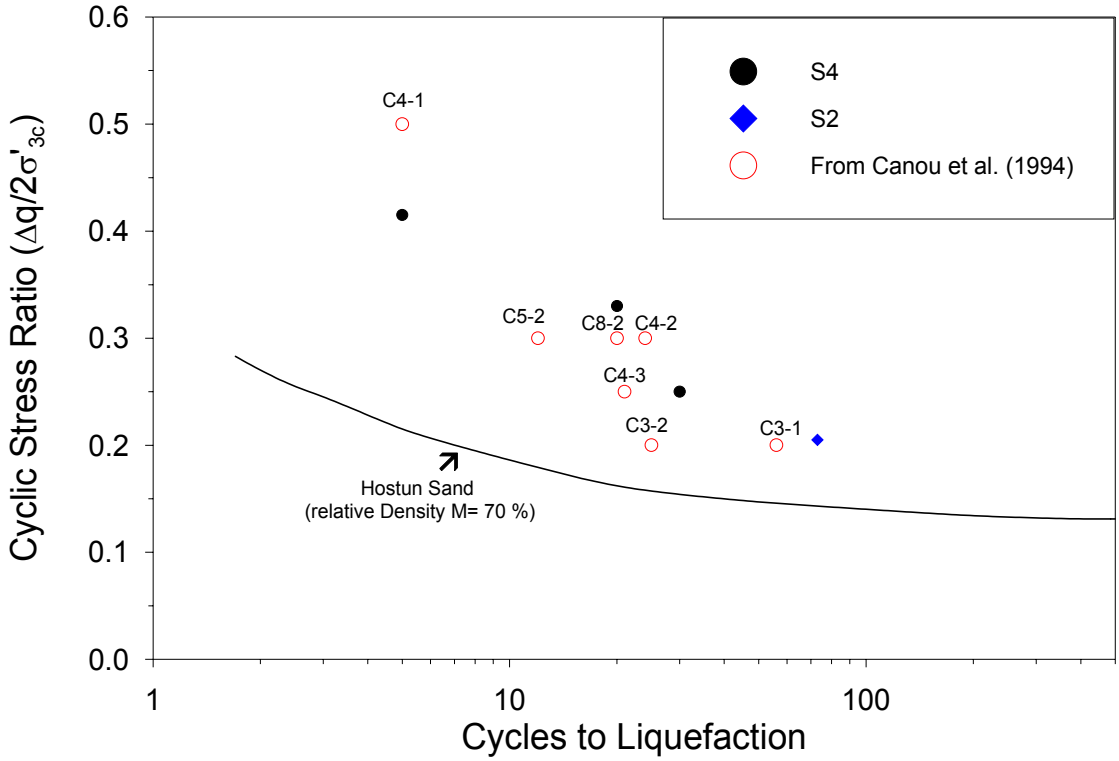

Figure 17. Cyclic resistance ratio as a function of the cycles to liquefaction (Nice slope).

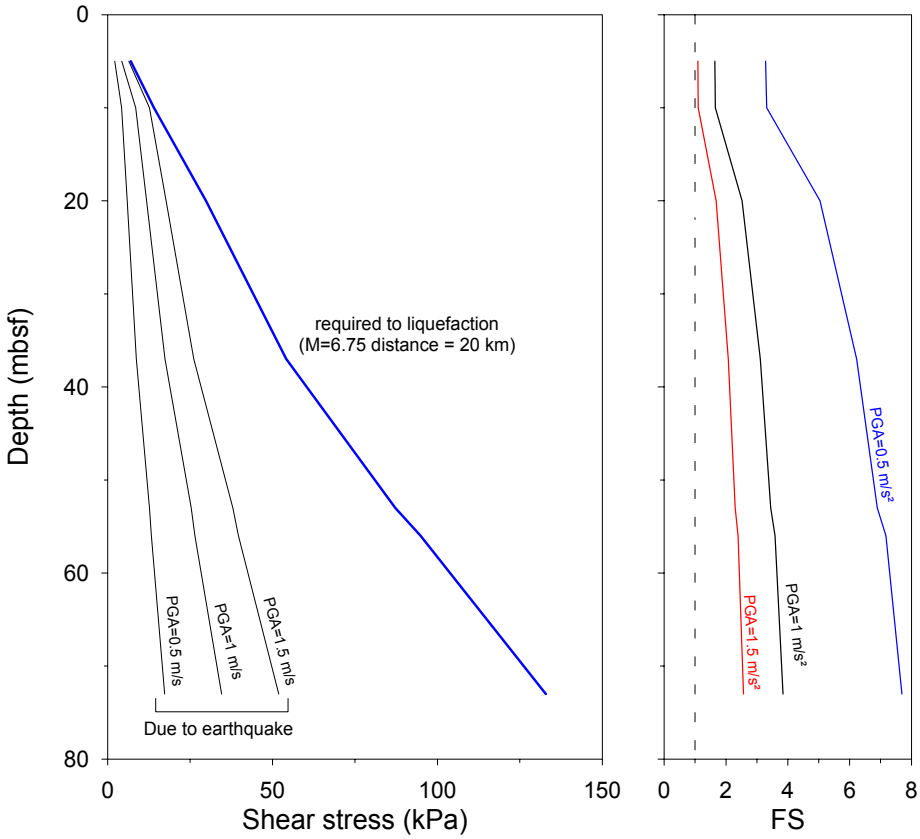

Figure 18. Analysis of the liquefaction susceptibility of the sediment layers from the Nice slope using the safety factor empirical method

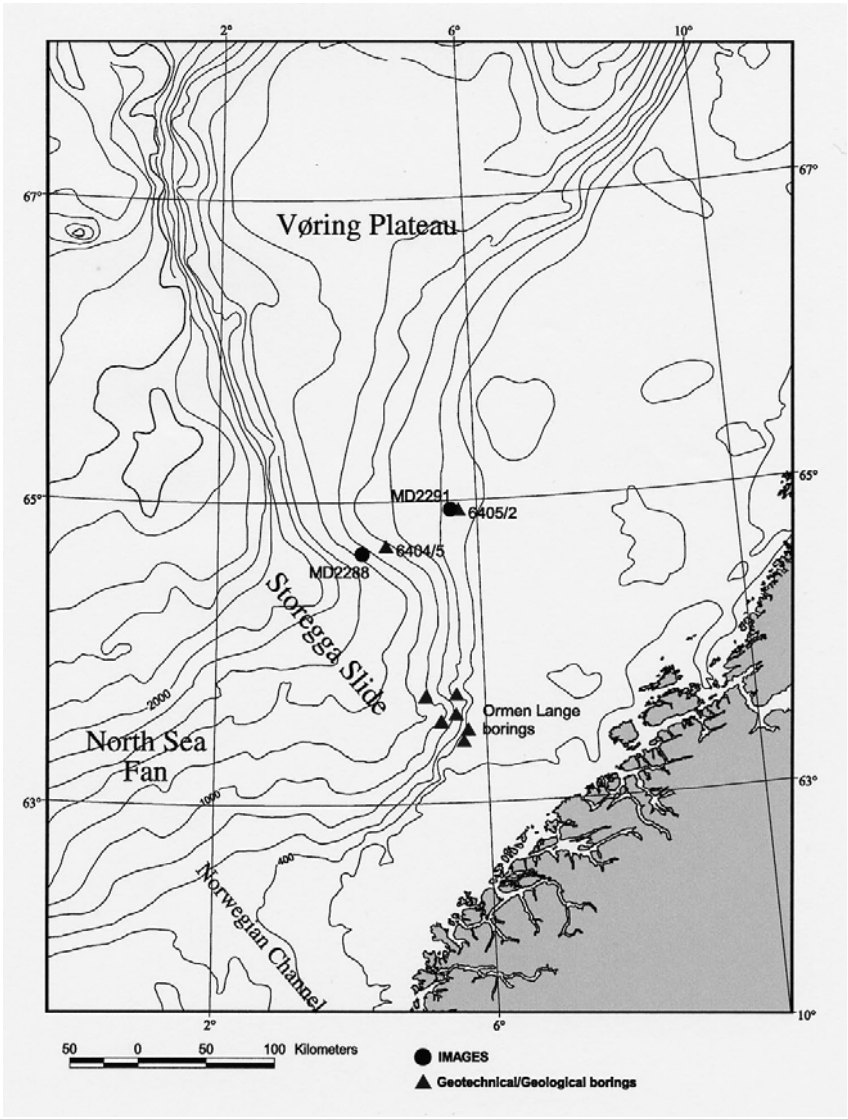

Figure 19. Bathymetry of the storegga slide including drill sites and boreholes location (B 6404/5, B 6405/2 and MD992288), where geotechnical data were made available by the Industry.

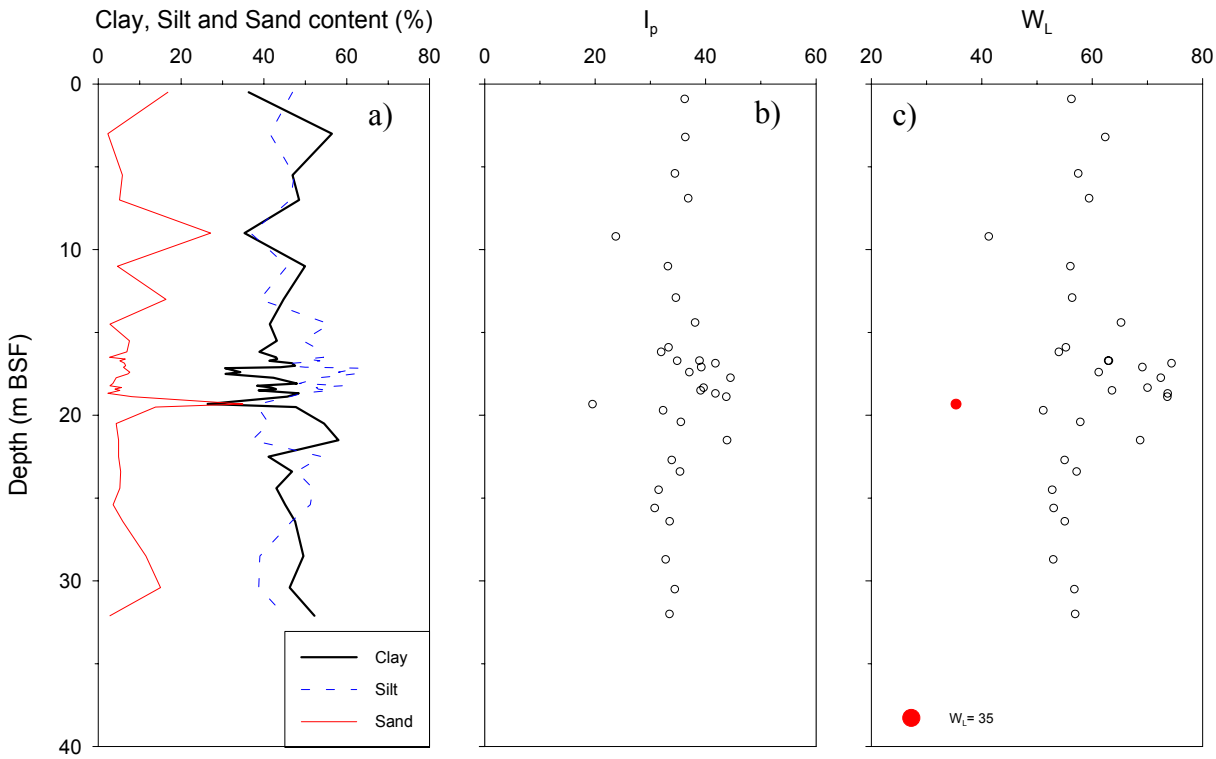

Figure 20. a) Grain size distribution b) plasticity index and c) Liquid limit versus depth below seabed - core MD99-2288.

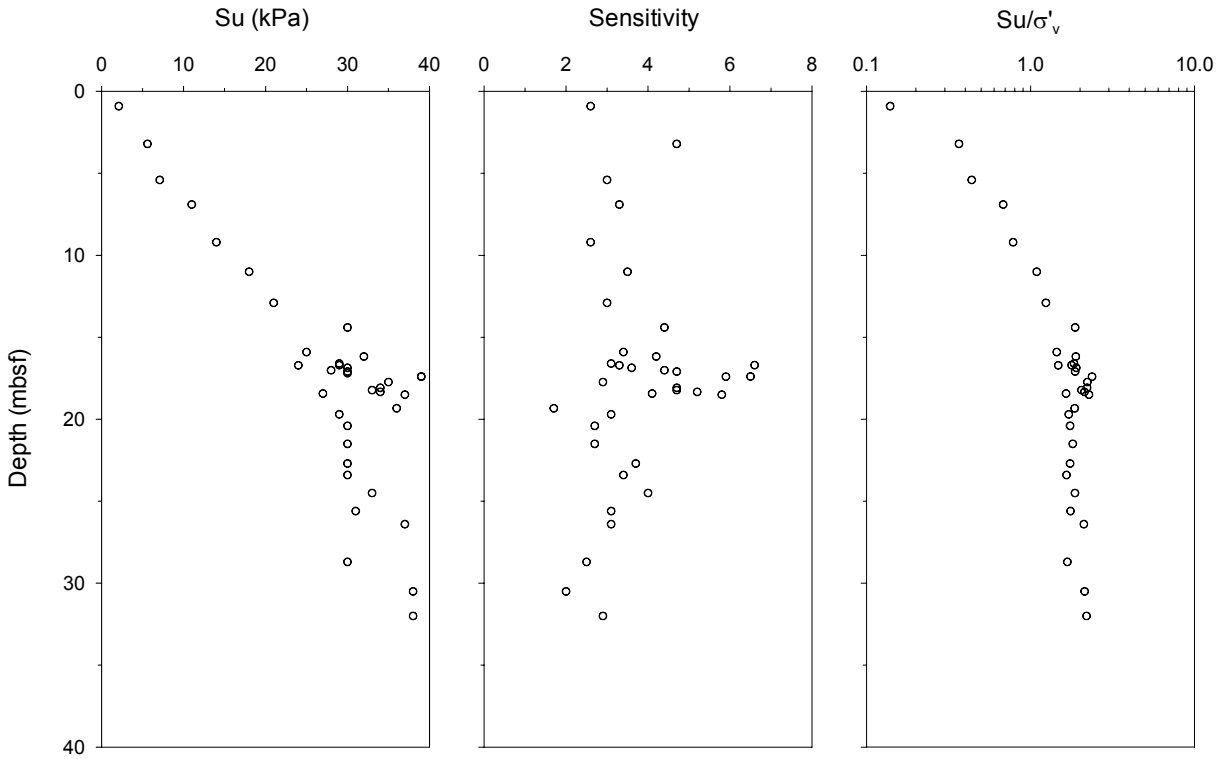

Figure 21. Undrained shear strength sensitivity and Su/σ'$_v$ profiles from MD99-2288.

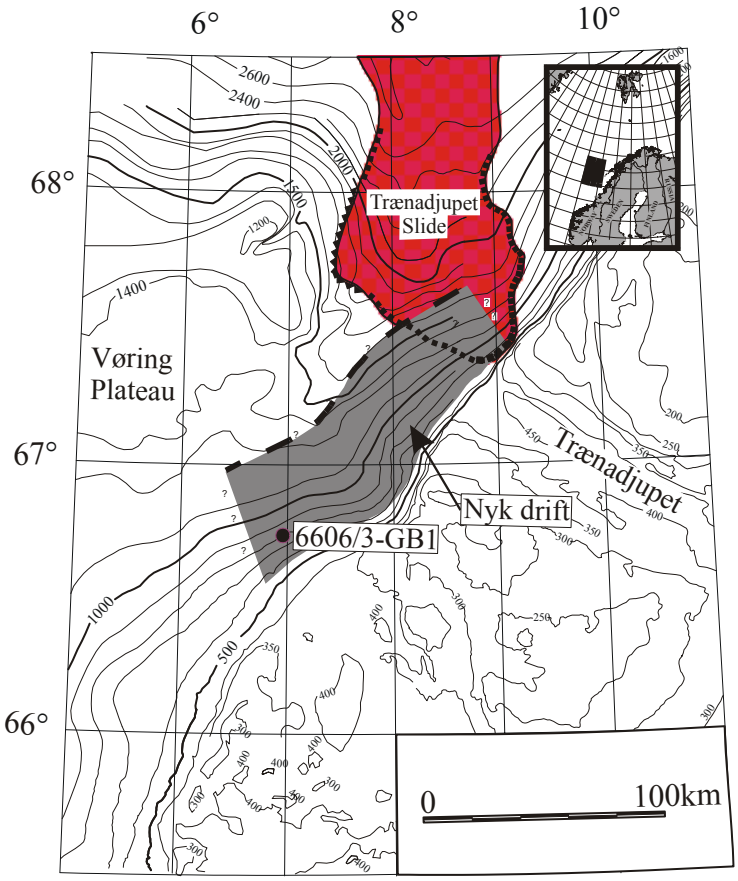

Figure 22. Bathymetric map including the location of the Trænadjupet Slide and the Nyk Contourite Drift. The location of borehole 6606/3-GB1 is shown.

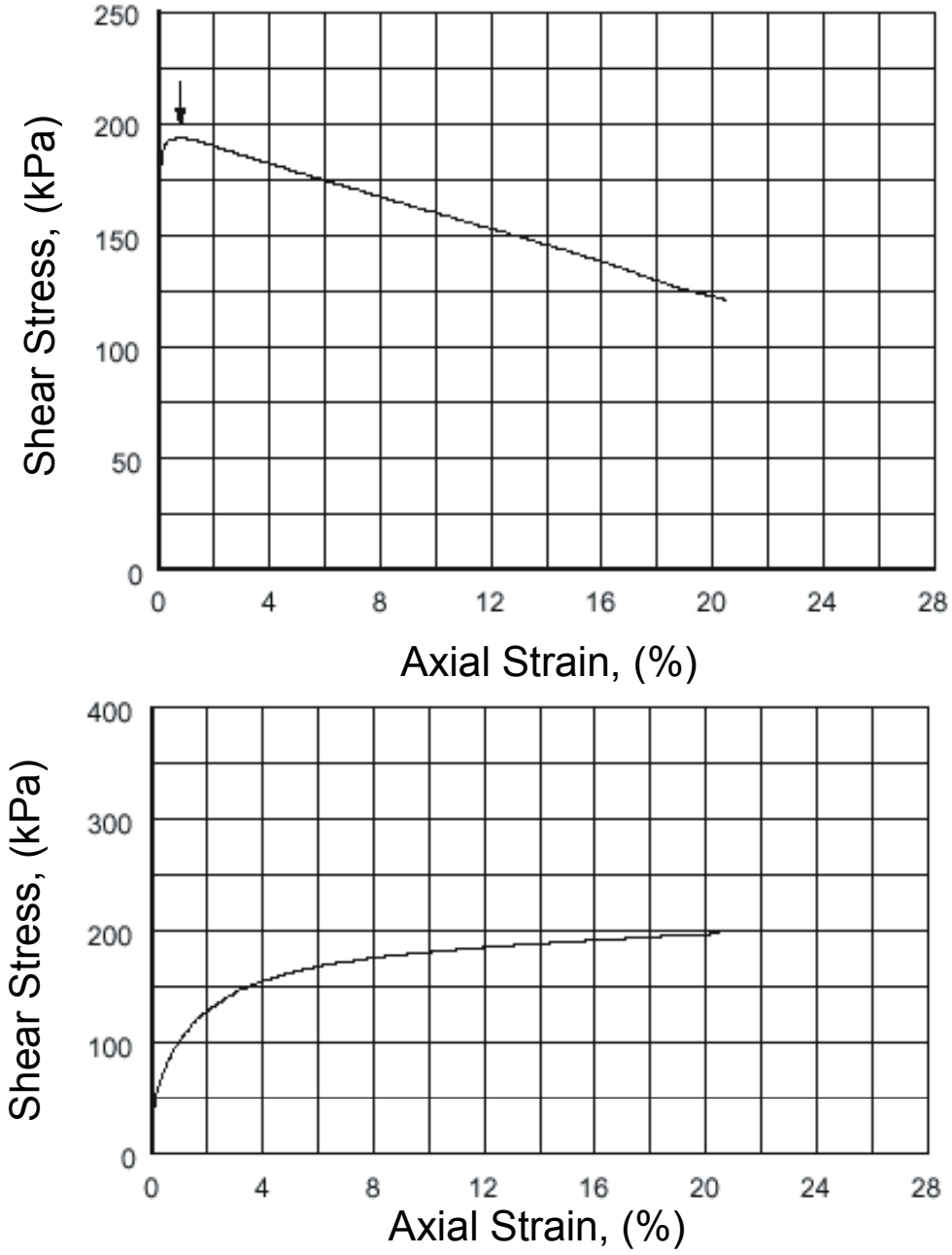

Figure 23. a) Shear stress versus axial strain and b) Pore pressure versus axial strain for the contouritic sediments sampled at 67.5 metre depth in borehole 6606/3-GB1.

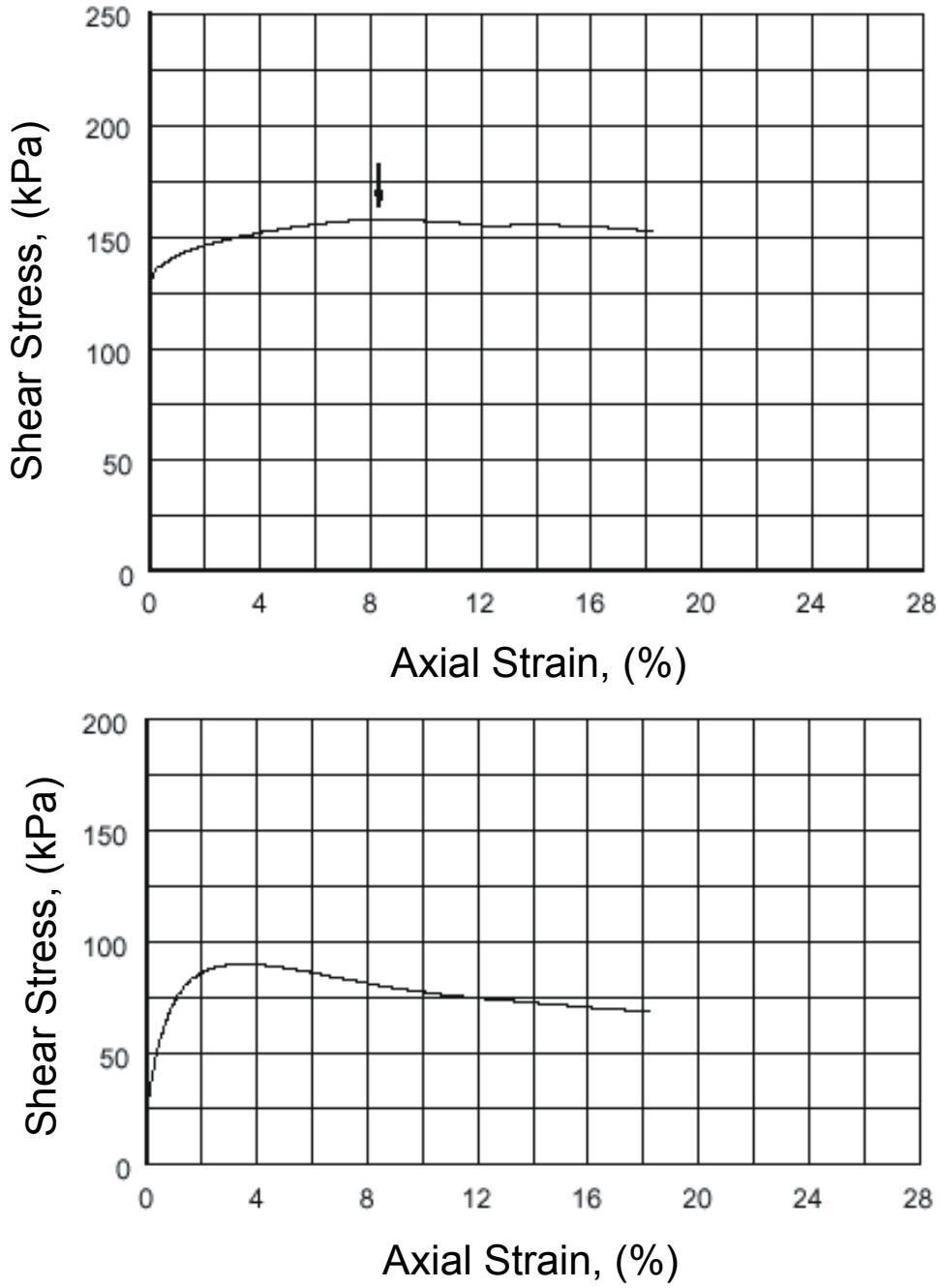

Figure 24. a) Shear stress versus axial strain and b) Pore pressure versus axial strain for the glacigenic sediments sampled at 40.2 metre depth in borehole 6606/3-GB1.